Eocene continental breakup in Baffin Bay

François Chauvet, Laurent Geoffroy, Hervé Guillou, René R, R.C. Maury, Bernard Le Gall, Arnaud Agranier, Adriano Viana

Eocene continental breakup in Baffin Bay

Authors

François Chauvet[a,b,*], Laurent Geoffroy[b1], Hervé Guillou[c2], René C. Maury[b], Bernard Le Gall[b], Arnaud Agranier[b] and Adriano Viana[d]

Affiliations

[a] *Univ Brest, IUEM, SEDISOR, Place Nicolas Copernic, 29280 Plouzané, France*

[b] *Univ Brest, CNRS, IUEM, UMR 6538 Laboratoire Géosciences Océan, Place Nicolas Copernic, 29280 Plouzané, France*

[c] *UMR 8212 Laboratoire des Sciences du Climat et de l'Environnement, LSCE/IPSL, CEA-CNRS-UVSQ, Université Paris-Saclay, F-91198 Gif-sur-Yvette, France*

[d] *Petrobras, Petróleo Brasileiro S.A., Rio de Janeiro, 1301E Brazil; E&P/UN-RIO/ATEX/ABIG-PL*

Contacts

* Corresponding author e-mail address: francois.chauvet@sedisor.eu (F. Chauvet)

laurent.geoffroy@univ-brest.fr (L. Geoffroy), herve.guillou@lsce.ipsl.fr (H. Guillou), rene.maury@univ-brest.fr (R. Maury), Bernard.legall@univ-brest.fr (B. Le Gall), arnaud.agranier@univ-brest.fr (A. Agranier), aviana@petrobras.com.br (A. Viana).

1 Tel.: +33 02 98 49 87 33

2 Tel.: +33 01 69 82 35 56

Keywords

- Baffin Bay opening
- West Greenland Volcanic Province

- Seaward Dipping Reflectors
- Volcanic passive margin
- $^{40}Ar/^{39}Ar$ and K-Ar dating
- Paleomagnetism

Abstract

We question the timing of continental breakup and early oceanization in Baffin Bay, North-East Atlantic. North of the Ungava fault zone, the breakup was syn-magmatic and led to the development of conjugate volcanic passive margins (VPMs). We investigated the innermost part of the W-Greenland VPM where a remarkable inner-SDR is fully exposed in the Svartenhuk area. Our new radiometric ages and paleomagnetic data from syn-tectonic basaltic lavas indicate that continental stretching and thinning spanned the C26r to, at least, the C24r period, giving an Eocene lower boundary age for continental breakup in Baffin Bay. These results contradict the proposed flooring of Baffin Bay by a Paleocene oceanic crust older than C24n and also question the accretion of oceanic crust before C22. We confront our results to the dynamics of the northward oceanic-rift propagation across the Ungava transform fault system, and we suggest that plate breakup in Baffin Bay occurred ~8 m.y. later than in N-Labrador Sea as a result of the thermal and mechanical barrier effect induced by the Ungava transform zone.

1. Introduction

The extinct Labrador-Baffin oceanic axis (Fig. 1) is part of a wide Phanerozoic divergent system including the NE-Atlantic Ocean, resulting from the Tertiary continental breakup of Eurasia, Greenland and North-America (Fig. 1a). On both sides of Greenland, the Paleogene plate breakup was preceded and accompanied by abnormal mantle melting (Saunders et al., 1997). The Labrador-Baffin axis is a typical example of oceanic rift propagation across an inherited transform fault (the Ungava fault zone) in connection with abnormal mantle melting. A recent analysis by Koopmann et al. (2014) suggested that early transform faults may act as rift propagation barriers and could enhance the amount of syn-breakup magmatism. We hereafter summarize the tectonic evolution of both the Labrador Sea and the Baffin Bay based on published data, as well as the related age uncertainties investigated in this study.

Following minor Late-Triassic to Late Jurassic magmatic dilatation (Watt, 1969; Larsen et al., 2009), the earliest synrift successions in the Labrador Sea are Early Cretaceous in age (Chalmers and Pulvertaft, 2001; Dickie et al., 2011; Jauer et al., 2015). They are represented by the volcanism of the Alexis formation and by wedge-shaped deposition of the Upper Bjarni and Appat sequence within the half grabens formed along the Labrador shelf (Fig. 2; see Chalmers, 2012 for a review). In the northern part of the Labrador Sea, a second episode of tectonic stretching spanned the Late Cretaceous until, possibly, the earliest Tertiary (Chalmers and Pulvertaft, 2001). Here, the oldest undisputed oceanic magnetic anomaly is C27n (Chalmers and Laursen, 1995), i.e. 62.2 – 62.5 Ma according to Ogg (2012). The "transitional" crust (Fig. 1c) bearing magnetic lineaments older than C27n has been modeled either as magma injected stretched continental crust (Chalmers, 1991, Chalmers and Laursen 1995), as slivers of stretched continental crust lying on exhumed serpentinized mantle (Chian and Louden, 1994) or as formed by slow seafloor spreading between C33 and C27 (Fig. 2; Strivastava and Roest, 1999).

The initial spreading directions were oriented ~N060E, i.e. sub-normal to the earlier continental rifted structures (Roest and Strivastava, 1989). Between C25 and C24, the oceanic fracture zones and magnetic anomalies indicate a major shift in kinematics in the Labrador Sea (Fig. 1). Spreading directions rotated from N060E to N010E (Roest and Strivastava, 1989; Fig. 1b). Oceanic spreading ceased in the Labrador Sea during the Oligocene (C13, Roest and Srivastava, 1989; Fig. 1a).

The SW-NE-trending left-lateral Ungava transform-fault system (UFS) connects the Labrador Sea to Baffin Bay (Fig. 1c). This area acted as a transtensive fault zone up to C25, becoming transpressive after C25 (Chalmers and Pulvertaft, 2001; Geoffroy et al., 2001; Suckro et al., 2013). Related folding structures are seismically well imaged on both sides of the Davis Strait High (Fig. 1c, e.g. Chalmers, 2012). The compressional deformation ceased in mid-Eocene times (Dalhoff et al., 2003).

Continental extension within Baffin Bay was also polyphase, defining an early continental sedimentary rift between Greenland and Baffin Island (Altenberndt et al., 2014; Gregersen et al., 2016; Fig. 1c). Extension would have also started during the Aptian-Albian (Kome Fm. in Fig. 2) and renewed in latest Campanian (see Dam et al., 2009 and Chalmers, 2012 for a review).

Linear gravity lows located in the central part of the Baffin Bay are interpreted as extinct spreading centers (Whittaker et al., 1997; Chalmers and Pulvertaft, 2001; Fig. 3a), but the offshore Baffin Bay depths are floored with non-interpretable magnetic anomalies (Fig. 3b). Crustal thicknesses and velocities from seismic refraction data are nevertheless consistent with the presence of oceanic crust in the deepest part of Baffin Bay (Fig. 1c; Keen et al., 1974; Suckro et al., 2012 ; Funck et al., 2012). Two major N-S-trending fracture zones in the basin (Fig. 3a) suggest also that oceanic spreading, if any, may have been coeval with the ~N-S reorientation of the kinematic trend in the Labrador Sea during the Eocene (Fig. 2; Geoffroy et al., 2001).

No absolute dating of any acknowledged oceanic crust exists in Baffin Bay, where there is no widely recognized pattern of linear magnetic anomalies (Fig. 3b). However, recent contributions (Oakey and Chalmers, 2012; Suckro et al., 2012; Hosseinpour et al., 2013) propose that oceanic-type crust of mid-Paleocene age (C27) would exist within the Baffin Bay. Oakey and Chalmers (2012) show that the pattern of transform faults in Baffin Bay is consistent with that of the Labrador Sea according to a common Euler rotation pole during the C24-C13 period. These authors state that older basement surrounding their postulated Eocene-Oligocene oceanic domain in the Baffin Bay is Paleocene. They further reinterpret shipborne magnetic profiles to reveal a Paleocene spreading center and associated magnetic anomalies, and thus draw limits for both Eocene and Paleocene oceanic crust domains in the Baffin Bay (Fig. 1c). However, none of the related studies takes into account the age of continental stretching recorded within the Baffin Bay continental passive margins.

A precise location of the continent-ocean boundary and a refined estimate of the age of the onset of continental extension and breakup in Baffin Bay are critical constraints to understand the dynamics of the propagation of continental breakup between Greenland and NAM plates from apart the Ungava fault zone (Fig. 1). In this contribution, we investigate from a detailed onshore study the precise timing of syn-magmatic continental extension along the SE-Baffin Bay passive margin in order to generate a time constraint on continental breakup and earliest oceanic accretion in Baffin Bay.

2. Geological setting

2.1. The volcanic passive margins

Volcanic passive margins (VPMs) are characterized by significant mantle melting and magma emplacement coeval with continental extension and final breakup (e.g. White et al., 1987). The upper-crustal section of conjugate VPMs is associated with two kinds of SDRs (Seaward-dipping seismic reflectors; Planke et al., 2000), both of them developing seaward with time: the inner SDR wedges and the outer SDR series (e.g. Planke et al., 2000; Franke et al., 2010). Inner-SDRs (Planke et al., 2000) represent wedges of syn-tectonic lavas developed over continentward-dipping detachment faults (e.g. Geoffroy, 2005; Quirk et al., 2014; Geoffroy et al., 2015). They represent the uppermost crustal section at VPMs and are clearly associated with continental stretching and thinning. They develop in the necking zones of VPMs (e.g. Geoffroy, 2005). The detachment faults bounding those inner-SDRs root at the top of a thick high-velocity lower crust (HVLC in Funck et al., 2016) of continental origin. This magma-injected lower crust shows a ductile behavior during crustal extension (e.g. Geoffroy et al., 2015; Clerc et al., 2015).

The interpretation of outer-SDRs is far more conjectural. No observable continentward-dipping faults bound outer-SDRs (e.g. McDermott et al., 2018). They form regular convex upward reflector sequences that deepen downward and merge along a planar low-dipping and seismically opaque area separating the extrusive sequences from the underlying mafic lower crust (Quirk et al, 2014; Type IIa in McDermott et al., 2018). The nature of the lower crust is unclear as there is insufficient data for an unequivocal characterization. Linear magnetic anomalies are recorded over domains covered with SDRs (e.g. Stica et al., 2014; Collier et al., 2017). Therefore, defining the continent-ocean boundary at the VPMs is a complex issue, as it could be located far away from the seaward limit of the necked part of the continental crust, i.e. within the so-called “oceanic crust domain” (Geoffroy et al., 2015).

2.2. The Baffin Bay VPMs

South of the Upernavik Escarpment (UE in Fig. 1c), the passive margins of Baffin Bay are volcanic passive margins (Geoffroy et al., 2001; Gregersen et al., 2013). Inner SDRs have been identified off SE Baffin Island and Central West Greenland (Fig. 1c; Skaarup et al., 2006; Block et al., 2012; Abdelmalak et al., 2018). Their age and along-strike extent are presently unknown. However, the inner part of the SE-Baffin Bay VPM is well-exposed in the Disko-Svartenhuk region, which is part of the so-called Western Greenland Volcanic Province (WGVP, Fig. 4). In this area, continental extension, coeval with regional magmatism, has never been dated with precision. Consequently, the timing of oceanic breakup in Baffin Bay is not constrained.

The WGVP corresponds to a variably thick pile of ultramafic to mafic lavas (from few hundred metres up to 7 km) crosscut by sheeted intrusions (e.g. Pedersen et al., 2002). The northern part of the WGVP represents the landwardmost exposure of the SE-Baffin Bay passive margin. In the inner part of the margin, the lava pile forms a flat-lying basaltic plateau up to 2 km thick. A crustal flexure has developed to the West, associated with a 4 to 7 km-thick lava wedge (Larsen and Pulvertaft, 2000). This wedge represents a syn-magmatic roll-over anticline developed over a major continentward-dipping normal fault, i.e. a fully-exposed inner-SDR (Geoffroy et al., 1998; 2001, Abdelmalak et al., 2012). The Arfertuarssuk Fault represents the master fault bounding the Svartenhuk SDR (Figs. 4 and 5).

2.3. Stratigraphy and previous dating

In agreement with former studies (e.g. Larsen and Grocott, 1992), we divided the Svartenhuk volcanic formations into four successive sequences (V1 to V4, from bottom to top) (Fig. 5). Our V1 and V2 formations correlate with the lower (subaqueous) and upper (subaerial) Vaigat picritic sequences, respectively. The V3 and V4 units correspond to the Svartenhuk and Naqerloq formations (Larsen et al., 2015), respectively (Fig. 4).

Recent $^{40}Ar/^{39}Ar$ datings are available from the Paleogene lava flows of W-Greenland (Larsen et al., 2015; Fig. 4a). The corresponding sampling was aimed at dating the Tertiary volcanic activity and was not focused on the timing relationships between magmatism and extension. Nevertheless, these data significantly improved the regional stratigraphic chart, based on former absolute datings and paleomagnetism (Figs. 4a and 4b; Storey et al., 1998; Riisager and Abrahamsen, 1999; Riisager et al., 2003).

According to these results, the ages of volcanic activity in W-Greenland span from C27n (late Paleocene) to C24r (Early Eocene). The earliest pulse is mid-Paleocene in age, spanning chrons 27n to 25r (Riisager and Abrahamsen, 1999; Riisager et al., 2003; Larsen et al., 2015), i.e. 62.5 to 57.7 Ma (after Ogg, 2012). Both Storey et al. (1998) and Larsen et al. (2015) suggest a hiatus of 1-2 m.y. or more at the end of this period (Fig. 4b). The second magmatic pulse, associated with transitional to alkaline basaltic successions, is dated back to 57-54 Ma, i.e. Early Eocene, during C24r (Storey et al., 1998; Riisager et al., 2003; Larsen et al., 2015). Early Eocene ages were also obtained for dykes crosscutting the Paleocene-related series in Disko and Nuussuaq (Storey et al., 1998) and in the Svartenhuk Peninsula (Geoffroy et al., 2001; Fig. 4).

2.4. Svartenhuk structure

The tectonics of the Svartenhuk inner-SDR has already been investigated (Geoffroy et al., 2001; Larsen and Pulvertaft, 2000). We present an original cross-section across the southern part of the Peninsula (Fig. 5). The Svartenhuk flexure (Fig. 6a) developed in the hanging wall of the Arfertuarssuk fault (Fig. 5). At a smaller scale, the subaerial V2-V3 successions are repeatedly downfaulted by normal faults, all of them facing the continent. Extensional fans are observed at all scales with lavas exhibiting an increase in dip with depth (Geoffroy et al., 2001). Internal angular unconformities are very common within the lava wedge. Southwestward, i.e. toward the ocean, the average dip of lavas tends to increase at sea level together with a progressive passive rotation to low dips of early syn-magmatic normal faults (Fig. 5; Fig. 6b). The eroded V4 unit is located at the top of the Svartenhuk wedge in apparent conformity with the V3 unit (Fig. 5, Fig. 6c-d). The V4 basalts are tilted seaward and downthrown (together with underlying V3 to V1 lava piles) against the Arfertuarssuk Fault (Fig. 5 and Fig. 6d).

The structural and stratigraphic architecture of the entire volcanic succession shows a seaward-migration of syn-magmatic extension (Geoffroy et al., 2001; Fig. 5). Another SDR appears to have developed westward of the Arfertuarssuk Fault (Fig. 5). Although available offshore seismic reflection data from this area are of poor penetration, we are confident that series of SDRs continue far offshore, like across the E-Greenland VPM (e.g. Dahl-Jensen et al., 1997; Brooks, 2011) and, elsewhere, across VPMs worldwide (e.g. Planke et al., 2000; Franke et al., 2010; Stica et al., 2014). SDRs are not only described far away from Svartenhuk in Baffin Bay (Suckro et al., 2012; Abdelmalak et al., 2018) but also along the conjugate Baffin Island VPM (Skaarup et al., 2006; Abdelmalak et al., 2018). As it represents the innermost part of the “syn-rift” formations of the SE-Baffin Bay passive margin, the Svartenhuk SDR offers a unique opportunity to assign a precise age to the SE-Baffin Bay margin continental extension.

3. Radiometric data

3.1. Sampling strategy

Selected rocks for radiometric dating were collected from 12 basaltic flows (Fig. 7a), one trachytic intrusion (S29-E2), 4 sills and 7 dykes (Fig. 7b). From the 12 flows (Fig. 7a), one sample came from V1 (S40-E1), 5 from V2, 2 from the lower V3 and 4 from the topmost V4 sequence. Reliable dating was precluded by the massive hydrothermal alteration of samples from the upper half of V3 above the Arfertuarssuk Fault. Among the 5 selected sills, one sill crosscuts the V2 unit (S22-H2), two crosscut the base of V3 (S36-E5 and S8-E13), another crosscuts the upper part of the V3 unit (S26-H1) and the trachytic intrusion (S29-E2) was emplaced between the V3 and V4 units. The sampled dykes show different trends and dips, some being parallel to the SDR flexure axis, while others are not (Geoffroy et al., 2001). Three dykes strike parallel to the NW-SE trending flexure and extensional faults (S40-E6, S14-H2, 23H4), and are thus considered to have been emplaced under the same stress field. The other dykes strike obliquely (S22H4, S27-E4) or are sub-normal (S20-E18, S2-E8) to the flexure axis (see the different directions of dykes in Fig. 7b).

3.2. Dating methods

With the exception of porphyritic trachyte S29-E2, dated on handpicked alkali feldspar phenocrysts, all datings were performed on the separated groundmass of the lavas. The techniques of groundmass separation and preparation are described in Guillou et al. (1998). All procedures concerning the sample preparation, as well as the unspiked K-Ar and ^{40}Ar-^{39}Ar methods, are detailed in the supplemental online material (Section methods).

New unspiked K-Ar ages are reported in Table 1a. Along with the radiometric dating, major element analyses were carried out to estimate the degree of alteration of selected samples and their groundmass. The loss-on-ignition values (L.O.I.) usually range from 0 to 2 wt.%. However, despite a thorough removal of secondary phases, the groundmass of the V2 unit picritic lavas yielded L.O.I. values spanning 2.5 to 5.1 wt.%. These values indicate that the corresponding lavas have undergone a pervasive alteration. Owing to the very low K contents and high modal abundance of olivine phenocrysts in these basalts, the ages obtained from the V2 samples were considered unreliable and excluded from our set of dating results (Fig. 7a).

Full analytical results of trachyte S29-E2 dating by the $^{40}Ar/^{39}Ar$ method are given in Suppl. Table 1. Step-heating $^{40}Ar/^{39}Ar$ plateau age data for groundmass samples are reported in Table 1b (with full analytical results in Suppl. Table 2). We were unable to obtain an age for sample S27-E12 because of alteration, and ages could not be determined for samples S33-E9 and S40-E1 because of recoil effects during irradiation. Only the one step-heating experiment (S35-E5) yielded concordant spectra with 100% of the gas defining age plateaus (Suppl. Fig. 1). The six other plateau ages were defined for gas release rates from 60 % to 87 % (Table 1b). The $^{40}Ar^*$ contents in samples S30-E1a, S30-E1b, S22-H4 and S21-H1 range from 68 % to 99 %, with typical values from 90 % to 99 % for the plateau steps. For samples S23-H4, S35-E5 and S42-E5, which are less potassium-rich than the others, $^{40}Ar^*$ ranges from 22 % to 90 %, with typical values of 60 % to 90 % for the plateau steps.

Plateau ages, isochron regressions and probability of fit estimates were calculated using ArArCalc (Koppers, 2002). The uncertainties on individual plateau ages as well as the inverse isochrons are given at 2σ (Suppl. Fig. 1, Table 1b). The $^{40}Ar/^{36}Ar$ intercept values defined for the associated isochrons are atmospheric, within the error bars. The total fusion ages are similar to the plateau or isochron ages when the margin of error is taken into account. This feature indicates that the effect of argon loss or excess argon is almost negligible for most samples. With the isochron approach, we make no assumption regarding the trapped component, and combine estimates of analytical precision and internal disturbance of the sample (scatter around the isochron). Therefore, the isochron ages (Table 1b) are preferred over the weighted mean plateau ages.

3.3. Analysis of results

The measured K-Ar ages range from 60.38 ± 1.34 to 53.85 ± 2.84 Ma, discarding the age of 63 Ma obtained on the highly olivine-phyric sill S36-E5 which crosscuts the V3 unit (Fig. 7b). The $^{40}Ar/^{39}Ar$ isochron ages and the unspiked K-Ar ages of samples S21-H1 and S35-E5 are equivalent at the 95 % confidence level (Fig. 7c). This comparison is useful to assess the reliability of the ages obtained via the unspiked K-Ar method. However, a comparison between Table 1a and 1b reveals some inconsistencies in the K-Ar data with respect to stratigraphic constraints as well as differences between K-Ar and $^{40}Ar/^{39}Ar$ ages (Fig. 7c and samples with asterisk * Table 1a).

For instance, the ^{40}Ar/^{39}Ar ages of 61.08 ± 0.56 Ma and 59.78 ± 0.41 obtained for the base of V2 (S42-E5) and for the base of V3 (S35-E5), respectively (Table 1), indicate that the youngest K-Ar ages of the stratigraphically lowermost samples S40-E1 (V1), as well as the V3-related sample S33-E9, are too young (Fig. 7c). This underestimation is most likely due to argon loss through glass hydration and alteration. Sample S36-E5 comes from a 15-m-thick highly porphyritic sill. Incomplete degassing of the magma prior to crystallisation might be a source of excess ^{40}Ar*, thus explaining the apparent old K-Ar age of ~ 63 Ma. For the topmost V4 succession, the ^{40}Ar/^{39}Ar ages of S30-E1 (54.39 ± 0.6 Ma) and S21-H1 (55.20 ± 0.79 Ma) are preferred to the older unspiked K-Ar ages of samples S30-E1, S30-E3 and S30-E4 (Figs. 7a-c).

The overestimation of the K-Ar ages is probably related to excess ^{40}Ar*, as shown from the step-heating experiments of S30-E1. We note that the 4 and 3 first increments from experiment A and B, respectively (Suppl. Fig. 1), when excluded from the plateau calculations, yield apparent ages significantly older than the plateau ages. This feature may be due to a component of extraneous argon in some aliquots.

The unspiked K-Ar and ^{40}Ar/^{39}Ar ages obtained for the Svartenhuk intrusive system are clustered into two main groups, Paleocene and Eocene. The Eocene K-Ar ages yielded by dykes and sills are consistent, at 2σ, with the ^{40}Ar/^{39}Ar isochron age of dyke S22-H4 (~ 54.4 ± 1 Ma, Table 1). The Paleocene K-Ar age yielded by dyke S40-E6 is consistent with the ^{40}Ar/^{39}Ar isochron ages of dyke 23-H4 (~59 ± 1 Ma). Most of the intrusions are Early Eocene, with ages spanning a wider range than for unit V4, from 57 to 53 Ma (Table 1). The dykes are either parallel (e.g. S14-H2) or oblique (e.g., S20-E18) to the flexure and clearly fed the eroded top of the SDR. Two dykes only (S40-E6 and S23-H4), striking parallel to the regional flexure, were emplaced synchronously with the Paleocene volcanic series.

4. Paleomagnetic data

4.1. Sampling

Samples for paleomagnetic studies were drilled in the V2 and V3 units, alongshore the southern coast of Svartenhuk. The V1 sequence was previously sampled to the East of Svartenhuk by Riisager et al. (2003) along a 200 m high continuous vertical section (profiles 3 & 4 on Fig. 4a). A total of 244 cores were drilled from 30 lava flows and 11 intrusions (Figs. 7a-b). Among the sampled flows, 19 were sampled within the V2 unit and the remaining 11 belong to the lower and upper parts of the V3 unit. All cores were drilled in the central part of the lava flows and dykes to minimize weathering effects and to avoid the thermal influence of overlying flows or nearby intrusions. The cloudy and foggy weather precluded the systematic use of a sun compass for orientation of the drilling cores. All measurements were corrected using the 2012 IGRF-based regional declination of -37°.

4.2. Methods

A total of 232 samples were stepwise thermally demagnetized. A "pilot demagnetization" was performed for one or two samples per flow/dyke with 15 successive steps to determine the thermal spectrum of each flow. These results show that the magnetic mineralogy is very stable over a large range of temperatures, while the Curie temperature is close to 580°C indicating that the main magnetic carrier phase is low-Ti magnetite (Fig. 8a-b).

Demagnetization was performed on 5 to 10 samples per flow/dyke (6 samples on average) using 12 to 14 steps, from room temperature up to a maximum of 600 °C (Suppl. Tables 3-4). Thermal demagnetization was conducted in air using a PYROX furnace with the heating space controlled by three separate heating coils with independently controlled thermocouples maintaining the thermal gradient under 2 °C at 500 °C over the entire heating zone. Cooling was obtained with air circulation over the samples in a magnetic field of less than 1 nT.

After each step, the samples were measured using a 755R-2G cryogenic magnetometer equipped with high homogeneity pick-up coils. Both the furnace and the magnetometer were housed within the mu-metal shielded room of LSCE Gif-sur-Yvette. Possible mineralogical changes during heating were monitored by measuring the low field susceptibility value after each thermal demagnetization step. The thermal demagnetization was stopped when less than 10 % of the initial Natural Remanent Magnetization (NRM) was left or when magnetic mineral changes occurred due to destabilization of the magnetization.

The final direction of the Characteristic Remanent Magnetization (ChRM) was determined using Principal Component Analysis (PCA) (Kirschvink, 1980), that allowed us to define the mean angular deviation (MAD, Suppl. Tables 3-4). In the great majority of cases, apart from a viscous component removed after the very first demagnetization step (100-140 °C), demagnetization diagrams indicated univectorial behaviors (Figs. 8c-8e). However, five samples from dyke S6A, six samples from dyke 27B and one sample from flow S6C displayed more complex demagnetization patterns and could not be interpreted (Fig. 8f). Overall, reliable results were obtained from 232 samples out of 244.

MAD values were lower than 5° for 226 samples, and ranged between 5 and 10° for the 6 remaining samples (Suppl. Tables 3-4). Mean-site directions calculated using Fisher's statistics were based on 3 to 7 independent ChRM directions (Suppl. Tables 5-6). Some of the ChRM directions could be excluded from the mean direction of individual flows as these data points were clearly outliers (Suppl. Tables 3). The mean-flow directions were defined with a precision angle α_{95} ranging from 2° to 10.7° with a mean value of 5° (Suppl. Tables 5; Suppl. Fig. 2). The results obtained from the dykes were more complicated. Two of the dykes (S27B and S6A) yielded a poorly defined mean direction with a precision angle α_{95} of 18° and 40°, respectively (Suppl. Table 4, Suppl. Fig. 3). The directions obtained from the other dykes were characterized by α_{95} values varying between 3.4° and 11° (Suppl. Table 4).

4.3. Data analysis

The new paleomagnetic dataset indicates that all the lava flows and intrusions from the Svartenhuk volcanic wedge were emplaced during a single or several distinct periods of reversed polarity of the magnetic field (Suppl. Table 5). Solely dyke S7A yielded a normal polarity ChRM (Suppl. Fig. 3; Suppl. Table 6). Our results are consistent with previous aeromagnetic results in this area (Rasmussen, 2002). After tilt correction, the resulting mean paleomagnetic direction of lava flows is Dec = 151.4°, Inc = -64.9° (n/N=30/30, α_{95} = 6.2°; Fig. 9a). The ChRM directions of the dykes are more scattered than those obtained from the flows (Fig. 9b). Restoring dykes to the vertical gives ChRM directions similar to those from the basaltic flows (Fig. 9b).

Our paleomagnetic mean directions for the untilted V2 and V3 lavas are very close to those obtained by Riisager et al. (2003) from the sub-horizontal V1 unit (Fig. 9). Incidentally, this indicates that the dip of lava flows within the SDR wedge is of tectonic origin and not due to paleo-slopes.

Plotting declinations and inclinations from the bottom to the top of the SDR reveals homogeneity (Fig. 9c). The ChRM directions show deviations less than 32° regarding the mean vector. The deviations in our data set could reflect short-time excursions of the geomagnetic field as otherwise suggested by Riisager et al. (2003).

5. Discussion

Our set of K-Ar and $^{40}Ar/^{39}Ar$ ages indicates that the Svartenhuk SDR lavas were emplaced between 61.5 and 54 Ma (Fig. 7c). According to Ogg's (2012) time scale, these ages suggest that the reversed magnetization inferred from our paleomagnetic data correspond to magnetochrons C26r and C24r (Fig. 10). These results are consistent with former data from the WGVP. The normal polarity interval recognized by Riisager and Abrahamsen (1999) in the basal Vaigat Formation at Vaigat Fjord (Fig. 4) would indicate that the Paleogene volcanic activity in the exposed WGVP spanned C27n to C24r (Storey et al., 1998; Riisager and Abrahamsen, 1999; Riisager et al., 2003; Skaarup and Pulvertaft, 2007; Larsen et al., 2015; Fig. 10). In Svartenhuk, the youngest (Eocene) ages are related to the V4 unit. Due to pervasive hydrothermal alteration we did not obtain reliable ages from the top of the Late Paleocene V3 unit. However, our datings bracket the eruption of the Vaigat picrites V2 between 61.5 and 59.5 Ma, i.e. during the Middle Paleocene (Selandian).

With the exception of early dykes S40E6 and S23H4, which were injected during the Paleocene, most of the sampled intrusions in Svartenhuk yielded early Eocene ages consistent with former observations in this area (Geoffroy et al., 2001) and farther south in Nuussuaq and Disko (Storey et al., 1998; Larsen et al., 2015, Fig. 10). Paleomagnetic results allow us to refine the age of those intrusions as being restricted to C24r (57-54 Ma; Ogg, 2012; Fig. 10).

The magmatic development of the inner SDR until the Eocene is of particular importance. Although a 1-2 m.y. pause in magmatic activity may have occurred during the development of the SDR wedge, the Svartenhuk SDR wedge developed throughout the Paleocene, until the Early Eocene. The V4 alkaline basalts appear to be coeval with the thick lava piles of enriched basalts recognized in western Nuussuaq and Hareøen Island (Kanísut Member) and in western Ubekendt Ejland (Nûk takisôq Member and Erqua Fm., Fig. 10). We investigated the structure of the oblique margin segment of Nuussuaq during several field trips (Geoffroy et al., 2001; Abdelmalak et al., 2012). The original sections from Fig. 11 clearly outline that the Eocene Kanisut Member (Larsen et al., 2015) is also part of the syn-tectonic magmatic wedge in Nuussuaq (Guan, 2018).

Normal-polarity basalts of probable C24n ages do exist offshore to the West of Nuussuaq and Ubekendt Ejland (Rasmussen, 2002; Fig. 3b). In addition, Eocene sub-aerial basalts, spanning C24r to C22r (~56.5 to ~50 Ma), have been drilled off W-Greenland (Delta-1 well, >110 km WSW of Svartenhuk Halvø, Fig. 1c; Nelson et al., 2015). These basalts present petrologic and geochemical affinities with the Eocene Kanisut and Svartenhuk V4 formations and they overlie the margin crustal necking zone (Hosseinpour et al., 2013; Suckro et al., 2012). In addition, SDRs have recently been imaged in the Central-East Baffin Bay 100 km seaward and 200 km to the NW of the Svartenhuk SDR (Abdelmalak et al., 2018; Fig. 1c). These SDRs are located close to the Delta 1 Eocene basalts (Fig. 1c), within the oceanic crust domain inferred to be Paleocene by Oakey and Chalmers (2012). The occurrence of SDRs of probable Eocene age in the central part of the Baffin Bay might lead to envision a larger volume and possibly an extended duration for the syn-rift magmatism.

As indicated by dyke orientations (e.g. Fig. 7b) and by stress-inversion of a large amount of reliable fault-slip data, the C24r period was associated with instability in the stress field at the scale of the WGVP, with a shift in the minimum stress $\sigma 3$ from N060E to N010E (Geoffroy et al., 2001; Abdelmalak et al., 2012). Our additional datings of dykes globally support this view, with the ~EW dykes being younger (Fig. 12). This stress field was coeval and consistent with the C24 kinematic change in the Labrador-Baffin system (Geoffroy et al., 2001). However, the NS crustal extension had a minor influence on the ongoing tectonic development of the SDR in the NE-SW trend. The related deformation is better expressed along NW-SE trending fjords, suggesting a reactivation of older structures of probable Cretaceous age. During our field and airborne surveys, we also observed some ~NW-SE dykes (associated with the N060E extensional regime) cross-cutting ~E-W dykes (associated with the N010E extensional regime). The syn-magmatic extensional stress regime with $\sigma 3$ trending N010E, which appeared later, was probably a transient phenomenon.

Since it is widely admitted that significant continental extension ceases at the onset of seafloor spreading, our results strongly question the previously proposed Paleocene age for the earliest oceanic accretion in the southern Baffin Bay (e.g. Oakey and Chalmers, 2012; Hosseinpour et al., 2013). The development of an inner SDR along the innermost part of the West Greenland volcanic margin during C24r is inconsistent with the occurrence of continental breakup in Baffin Bay before C24n. More recent SDRs of possible C22 age (see above) are observed offshore in the Baffin Bay suggesting that continental breakup could be much younger than C24n. By comparing the SDR observations of Block et al. (2012), Suckro et al. (2012) and Abdelamalak et al. (2018), located ~180 km off Svartenhuk, and nearby Delta-1 observations of subaerial basalts (Fig. 1c; Nelson et al., 2015), we infer that the crust in this area was buoyant and thicker than any normal oceanic crust, and therefore of possible continental affinity.

The present-day knowledge of the crustal architecture on the southern Baffin Bay passive margins is exclusively based on two refraction profiles striking at a high angle to the crustal thinning gradient (profiles 4 and 5 in Fig. 1c). Unfortunately, no seismic refraction or wide-angle seismic reflection lines were shot along the dip of the exposed W-Greenland VPM (Geoffroy et al., 2001). In Baffin Bay, the potential oceanic crust domain, i.e. the area without recognized SDRs (inner or outer) and with a constant oceanic-type crustal thickness in the range of 7.1 ± 0.8 km (White et al, 1992), is very limited. Figure 13 displays the results of two distinct and recent inversions for crustal thickness in Baffin Bay (Hosseinpour et al., 2013 and Welford et al., 2018). The oceanic-type crust (thickness lower than 8 km) is restricted to two small domains lying at the NW and SE tips of the main Baffin Bay transform, respectively. These domains are considerably more restricted in size than those formerly suggested (Oakey and Chalmers, 2012) and reported in Fig. 13a. We infer that the age of the oceanic crust in Baffin Bay, where it exists, ranges from C24n to C13 or, much more probably, from C22 to C13.

We consequently suggest that the oceanic-type floor in Baffin Bay is considerably narrower than previously proposed, with an accretion period limited to a max. ~20 m.y. time span. According to this interpretation, the southern Baffin Bay opened ca. 8 Ma after the proposed earliest oceanic accretion in the northern Labrador Sea and also after the N060E to NS kinematic reorganisation between North America and Greenland.

Such a diachronism in oceanic rift propagation from the N-Labrador Sea to Baffin Bay could be the result of the thermal and mechanical barrier effect caused by the Ungava transform zone (Fig. 1). Koopman et al. (2014) developed a numerical model suggesting that rift-parallel mantle flow is delayed at transform faults in segmented breakup systems. Transforms would act as rift-propagation barriers and would enhance considerably the amount of syn-breakup magmatism at the tip of the propagating rift. Funk et al. (2007) demonstrated the occurrence of high velocity igneous lower crust 4 to 8 km-thick (7.4 km/s) beneath the Ungava fault zone itself. These authors considered that the Ungava leaky transform zone would have acted as a barrier guiding the migration of hot material towards both the adjacent northern Labrador Sea and southern Baffin Bay VPMs.

Our data confirm that the Ungava fault zone acted as a mechanical barrier to the Labrador axis propagation for at least 8 m.y. (see above). However, the passive margins south of the Ungava fault zone appear to be less magma-rich (e.g. Peace et al., 2016) than those located to the north. These observations contradict part of the outcomes of Koopmann et al. (2014). Instead, our results suggest that mantle melting occurred on both sides of the Ungava fault zone and was possibly coeval with oceanic accretion to the south (N-Labrador Sea) and continental extension to the north (Baffin Bay) of this fault zone. The origin of this magmatism is beyond the scope of this paper. However, higher mantle temperature to the north of the Ungava fault zone (and possibly beneath it) and/or higher mantle fertility in the area may have enhanced mantle melting. In addition, we note that there is a very sharp transition from volcanic to non-volcanic passive margins to the north of the conspicuous Upernavik escarpment (UE in Fig. 1c; Whittaker et al. 1997). This escarpment bounds southwards the preserved Rae Archean lithosphere from a basement reworked during the Paleoproterozoic (Henriksen et al., 2009). This major NE-SW structure within the Baffin Bay could have played a significant role in the localization of asthenospheric melting at depth.

Conclusions

Volcanic activity in Svartenhuk was coeval with the tectonic development of the innermost SDR of the SE-Baffin Bay VPM. Our paleomagnetic and unspiked K-Ar and Ar-Ar dating results show that post-Mesozoic continental extension spanned the Paleocene until the Eocene (C24r). The inner position of the Svartenhuk SDR suggests that it recorded the earliest extension stage with regards to the seaward development of the VPM through time. Therefore, given the additional data from the Delta-1 well and available seismic data (Abdelmalak et al., 2018), we infer that oceanic accretion in Baffin Bay started certainly after C24r and probably as late as C22. All oceanic spreading operated with a ~NS trend. Admitting that seafloor spreading stopped at C13 (Roest and Strivastava, 1989; Oakey and Chalmers, 2012), the Baffin Bay oceanic stage would have lasted 20 m.y., from 50 Ma to 30 Ma. The Ungava fault zone acted as a barrier for oceanic rift propagation but not as a boundary for mantle melting. We suggest that the Upernavik discontinuity (and its prolongation to the East of Baffin Island) could have influenced the dynamics of mantle melting and magma output in the crust.

Targeted marine surveys on both sides of Greenland are required to better define the continent-ocean transitions in the NE-Atlantic and Baffin Bay basins. Such constraints are essential for a better understanding of continent-ocean boundaries at magma-rich passive margins and, at a wider scale, to improve our knowledge of the geodynamics of continental breakup between the NAM and Eurasia plates.

Acknowledgments

We would like to thank Catherine Kissel (Research Scientist at the French Atomic Energy Commission) and Camille Wandres (Assistant engineer at the Université de Versailles Saint Quentin) who performed the paleomagnetic analyses in the LSCE (Laboratoire des Sciences du Climat et de l'Environnement, CEA/CNRS/UVSQ). We are also indebted to J.L. Joron (Lab. P. Süe, CEA Saclay), who performed the irradiations of the samples for $^{40}Ar/^{39}Ar$ dating and to Sébastien Nomade and Vincent Sacao who performed the radiometric measurements. We are very grateful to Céline Liorzou and Philippe Nonnotte in Brest, for their help in the field and during sample preparation and major element measurements. The authors also thank Kim Welford for having kindly shared her results. The field work was carried out during a five-week expedition in the summer of 2012 and benefited from the high-quality logistic support of the research vessel Porsild from the Arctic Station in Godhavn (Greenland) and the polar yacht Vagabond. We are very grateful to the crews of the Porsild and to the Vagabond family, who provided pleasant and efficient assistance, both at sea and in the field. This work is part of the UBO-PETROBAS Volcabasin Project. We heartily thank two anonymous reviewers and editor Philippe Agard who provided thoughtful and constructive comments on the manuscript.

References

Abdelmalak, M.M., Geoffroy, L., Angelier, J., Bonin, B., Callot, J.P., Gélard, J.P., Aubourg, C., 2012. Stress fields acting during lithosphere breakup above a melting mantle: A case example in West Greenland. Tectonophysics 581, 132–143.

Abdelmalak, M.M., Planke, S., Polteau, S., Hartz, E.H., Faleide, J.I., Tegner, C., Jerram, D.A., Millett, J.M., Myklebust, R., 2018. Breakup volcanism and plate tectonics in the NW Atlantic. Tectonophysics, https://doi.org/10.1016/j.tecto.2018.08.002

Altenbernd, T., Jokat, W., Heyde, I., Damm, V., 2014. A crustal model for northern Melville Bay, Baffin Bay. J. Geophys. Res. 119, 8610–8632.

Block, M., Damm, V., Ehrhardt, A., Berglar, K., Schnabel, M., Altenbernd, T., 2012. Characteristics of the West Greenland Margin in the Southern Baffin Bay. 74th EAGE Conference & Exhibition, Abstract, 10.3997/2214-4609.20148225.

Brooks, C.K., 2011. The East Greenland rifted volcanic margin. Geol. Surv. Den. Green. Bull. 24, 96 pp.

Chalmers, J.A., 1991. New evidence on the structure of the Labrador Sea/Greenland continental margin. J. Geol. Soc. Lond. 148, 899–908.

Chalmers, J.A. and Laursen, K.H., 1995. Labrador Sea: The extent of continental and oceanic crust and the timing of the onset of seafloor spreading. Mar. Petrol. Geol. 12, 205–217.

Chalmers, J. and Oakey, G., 2007. Cretaceous-Palaeogene development of Labrador Sea and Davis Strait. poster A0048 presented at Annual Assembly, Eur. Geosci. Union, Vienna.

Chalmers, J. and Pulvertaft, T., 2001. Development of the continen tal margins of the labrador sea: A review. Geol. Soc. London Spec. Publ. 187, 77–105.

Chalmers, J. 2012. Labrador Sea, Davis Strait and Baffin Bay. Regional Geology and Tectonics: Phanerozoic Passive Margins, Cratonic Basins and Global Tectonic Maps, 1st Edition. Elsevier doi:10.1016/B978-0444-56357-6.00010-x.

Chian, D., Louden, K.E., 1994. The continent-ocean crustal transition across the southwest Greenland margin. J. Geophys. Res. 99, 9117–9135.

Clerc, C., Jolivet, L., Ringenbach, J.-C., 2015. Ductile extensional shear zones in the lower crust of a passive margin. Earth and Planetary Science Letters, 431, 1–7.

Collier, J. S., McDermott, C., Warner, G., Gyori, N., Schnabel, M., McDermott, K., & Horn, B. W., 2017. New constraints on the age and style of continental breakup in the South Atlantic from magnetic anomaly data. Earth and Planetary Science Letters, 477, 27–40. https://doi.org/10.1016/j.epsl.2017.08.007

Dahl-Jensen, T., Holbrook, W. S., Hopper, J. R., Kelemen, P. B., Larsen, H. C., Detrick, R., Bernstein, S., Kent, G., 1997. Seismic investigation of the east Greenland volcanic rifted margin. Geology of Greenland Survey Bulletin 176, 50–54.

Dalhoff, F., Chalmers, J.A., Gregersen, U., Nøhr-Hansen, H., Rasmussen, J.A., Sheldon, E., 2003. Mapping and facies analysis of Paleocene–Mid-Eocene seismic sequences, offshore southern West Greenland Labrador Sea: the extent of continental and oceanic crust and the timing of the onset of seafloor spreading. Marine Petrol. Geol. 20, 935–986.

Dam, G., Pedersen, G.K., Sønderholm, M., Midtgaard, H.M., Larsen, L.M., Nøhr-Hansen, H., Pedersen, A.K., 2009. Lithostratigraphy of the Cretaceous–Paleocene Nuussuaq Group, Nuussuaq Basin, West Greenland. Geological Survey of Denmark and Greenland Bulletin, 19, 171 pp.

Dickie, K., Keen, C.E., Williams, G.L., Dehler, S.A., 2011. Tectonostratigraphic evolution of the Labrador margin, Atlantic Canada. Marine and Petroleum Geology 28, 1663-1675.

Franke, D., Ladage, D., Schnabel, M., Schreckenberger, B., Reichert, C., Hinz, K., Paterlini, M., de Abelleyra, J., Siciliano, M., 2010. Birth of a volcanic margin off Argentina, South Atlantic. Geochem. Geophys. Geosyst., 11, Q0AB04, doi:10.1029/2009GC002715.

Funck, T., Erlendsson, Ö., Geissler, W. H., Gradmann, S., Kimbell, G. S., McDermott, K., & Petersen, U. K., 2016. A review of the NE Atlantic conjugate margins based on seismic refraction data. Geological Society, London, Special Publications, 447(1), 171–205. https://doi.org/10.1144/SP447.9

Funck, T., Gohl, K., Damm, V., Heyde, I., 2012. Tectonic evolution of southern Baffin Bay and Davis Strait: Results from a seismic refraction transect between Canada and Greenland. J. Geophys. Res., 117, B04107, doi:10.1029/2011JB009110.

Funck, T., Jackson, H., Louden, K., Klingelhöfer, F., 2007. Seismic study of the transform-rifted margin in Davis Strait between Baffin Island (Canada) and Greenland: What happens when a plume meets a transform-art. J. Geophys. Res.-Sol. Ea. 112, B04402, doi:10.1029/2006JB004308.

Geoffroy, L., 2005. Volcanic passive margins. C. R. Geoscience 337, 1395–1408.

Geoffroy, L., Burov, E.B., Werner, P., 2015. Volcanic passive margins: another way to break up continents. Nature Scientific Reports 5, 14828; doi: 10.1038/srep14828.

Geoffroy, L., Callot, J.P., Scaillet, S., Skuce, A.S., Gélard, J.-P., Ravilly, M., Angelier, J., Bonin, B., Cayet, C., Perrot-Galmiche, K., Lepvrier, C., 2001. Southeast Baffin volcanic margin and the North American–Greenland plate separation. Tectonics 20, 566–584.

Geoffroy, L., Gélard, J.P., Lepvrier, C., Olivier, P., 1998. The coastal flexure of Disko (West Greenland), onshore expression of the oblique reflectors. Journal of the Geological Society (London) 155, 464–473.

Gerlings, J., Funck, T., Jackson, H. R., Louden, K. E., Klingelhöfer, F., 2009. Seismic evidence for plume-derived volcanism during formation of the continental margin in southern Davis Strait and northern Labrador Sea. Geophys. J. Int., 176, 980–994.

Gregersen, U., Hopper, J.R., Knutz, P.C., 2013. Basin seismic stratigraphy and aspects of prospectivity in the NE Baffin Bay, Northwest Greenland. Marine and Petroleum Geology 43, 1-18.

Gregersen, U., Knutz, P.C., Hopper, J.R., 2016. New geophysical and geological mapping of the eastern Baffin Bay region, offshore West Greenland. Geological Survey of Denmark and Greenland Bulletin 35, 83-86.

Guan, H., 2018. Les marges passives volcaniques : origine, structure et développement. Ph.D. Thesis, Univ. de Bretagne Occidentale.

Guillou, H., Carracedo, J.C., Day, S., 1998. Dating of the upper Pleistocene-Holocene volcanic activity of La Palma using the unspiked K-Ar technique. J. Volc. Geotherm. Res. 86 (1-4), 137-149.

Henriksen, N., Higgins, A.K., Kalsbeek, F., Pulvertaft, T.C. 2009. Greenland from Archean to Quaternary. Geological Survey of Denmark and Greenland Bulletin 18, pp.126.

Hosseinpour, M., Müller, R.D., Williams, S.E., Whittaker J.M., 2013. Full-fit reconstruction of the Labrador Sea and Baffin Bay. Solid Earth, 4, 461–479.

Jauer, C.D., Oakey, G.N., Williams, G., Hans Wielens, J.B.W., 2015. Saglek Basin in the Labrador Sea, east coast Canada; stratigraphy, structure and petroleum systems. Bull. of Canadian Petrol. Geol. 62(4), 232-260.

Keen, C.E., Keen, M.J., Ross, D.I. Lack, M., 1974. Baffin Bay: small ocean basin formed by seafloor spreading. AAPGB 58(6), 1089-1108.

Keen, C.E., Dickie, K., Dehler, S. A., 2012. The volcanic margins of the northern labrador sea: Insights to the rifting process. Tectonics, 31, TC1011, doi:10.1029/2011TC002985.

Kirschvink, J.L., 1980. The least square lines and plane analysis of palaeomagnetic data. J. Roy. Astron. Soc. 62, 319-354.

Koopmann, H., Brune, S., Franke, D., Breuer, S., 2014. Linking rift propagation barriers to excess magmatism at volcanic rifted margins. Geology 42 (12), 1071–1074.

Koppers, A.A.P., 2002. ArAr CALC-software for 40Ar/39Ar age calculations. Computer and Geosciences 28, 605-619.

Larsen, H.C. and Saunders, A.D., 1998. Tectonism and volcanism at the SE Greenland rifted margin: a record of plume impact and later continental rupture. Proc. ODP Sci. Results 152, 503-533.

Larsen, J.G., 1983. Geologisk kort over Grønland, 1:100 000, Igdlorssuit, 71 V.1 Syd. København: Grønlands Geologiske Undersøgelse (English legend).

Larsen, J.G. and Grocott, J., 1992. Geologisk kort over Grønland, 1:100 000, Svartenhuk, 71 V.1 Nord. København: Grønlands Geologiske Undersøgelse (English legend).

Larsen, J.G. and Pulvertaft, T.C.R., 2000. The structure of the Cretaceous–Palaeogene sedimentary-volcanic area of Svartenhuk Halvø, central West Greenland. Geology of Greenland Survey Bulletin, 188.

Larsen, L.M., Heaman, L.M., Creaser, R.A., Duncan, R.A., Frei, R., Hutchison, M., 2009. Tectonomagmatic events during stretching and basin formation in the Labrador Sea and the Davis Strait: evidence from age and composition of Mesozoic to Palaeogene dyke swarms in West Greenland. Journal of the Geological Society, London, Vol. 166, 2009, pp. 999–1012. doi: 10.1144/0016-76492009-038.

Larsen L.M., Pedersen, A.K., Tegner, C., Duncan, R.A., Hald, N., Larsen, J.G., 2015. Age of Tertiary volcanic rocks on the West Greenland continental margin: volcanic evolution and event correlation to other parts of the North Atlantic Igneous Province. Geol. Mag., doi:10.1017/S0016756815000515.

Meyer, B., Chulliat, A., Saltus, R., 2017. Derivation and error analysis of the earth magnetic anomaly grid at 2 arc min resolution version 3 (EMAG2v3). Geochemistry, Geophysics, Geosystems, 18, 4522–4537. https://doi.org/10.1002/2017GC007280

McDermott, C., Lonergan, L., Collier, J.S., McDermott, K.G., Bellingham, P., 2018. Characterization of seaward-dipping reflectors along the South American Atlantic margin and implications for continental breakup. Tectonics, 37, 3303–3327. https://doi.org/10.1029/2017TC004923

Nelson, C.E., Jerram, D.A., Clayburn J.A.P., Halton, A.M., Roberge, J., 2015. Eocene volcanism in offshore southern Baffin Bay. Marine and Petroleum Geology 67, 678-691.

Oakey, G. N. and Chalmers, J. A., 2012. A new model for the Paleogene motion of Greenland relative to North America: Plate reconstructions of the Davis Strait and Nares Strait regions between Canada and Greenland, J. Geophys. Res.-Sol. Ea., 117, B10401, doi:10.1029/2011JB008942.

Ogg, J.G., 2012. Geomagnetic Time Scale. In: In: Gradstein, F.M., Ogg, J.G., Schmitz, M. and Ogg, G. (eds), The Geologic Time Scale 2012. Elsevier, Amsterdam, 85-113.

Peace, A., McCaffrey, K.J.W., Imber, J., Phethean, J., Nowell, G., Gerdes, K. & Dempsey, E., 2016. An evaluation of Mesozoic rift-related magmatism on the margins of the Labrador Sea: implications for rifting and passive margin asymmetry. Geosphere, 12(6), 1701–1724.

Pedersen, A.K., Larsen, L.M., Riisager, P., Dueholm, K.S., 2002. Rates of volcanic deposition, facies changes and movements in a dynamic basin: the Nuussuaq Basin, West Greenland, around the C27n-C26r transition. In: Jolley, D. W. and Bell, B.R. (eds) The North Atlantic Igneous Province: Stratigraphy, Tectonic, Volcanic and Magmatic Processes. Geological Society, London, Special Publications, 197, 157-181.

Planke, S., Symonds, P.A., Alvestad , E., Skogseid, J., 2000. Seismic volcanostratigraphy of large-volume basaltic extrusive complexes on rifted margins. J. of Geophys. Res. 105, 19335–19351.

Quirk, D.G., Shakerley, A., Howe, M.J., 2014. A mechanism for construction of volcanic rifted margins during continental breakup. Geology, v. 42, 12, 1079–1082.

Rasmussen, T.M. 2002. Aeromagnetic survey in central West Greenland: project Aeromag 2001. Geology of Greenland Survey Bulletin 191, 67-72.

Riisager, P. and Abrahamsen, N., 1999. Magnetostratigraphy of Palaeocene basalts from the Vaigat Formation of West Greenland. Geophysical Journal International, 137, 774-782.

Riisager, J., Riisager, P., Pedersen, A.K., 2003. Paleomagnetism of large igneous provinces: Case-study from West Greenland, North Atlantic igneous province, Earth Planet. Sci. Lett. 214, 409–425.

Roest, W.R. and Srivastava, S.P., 1989. Seafloor spreading in the Labrador Sea: A new reconstruction. Geology, 17, 1000–1004.

Sandwell, D.T., Müller, R.D., Smith, W.H.F., Garcia, E., Francis, R., 2014. New global marine gravity model from Cryo-Sat-2 and jason-1 reveals buried tectonic structure. Science, 346, 6205, 65-67, doi: 10.1126/science.1258213.

Saunders, A.D., Fitton, J.G., Kerr, A.C., Norry, M.J., Kent, R.W., 1997. The North Atlantic Igneous Province. In: Mahoney, J.J. and Coffin, M.F. (eds): Large igneous provinces. Geophys. Monograph 100, Amer. Geophys. Union, 45-93.

Skaarup, N. and Pulvertaft, T.C.R., 2007. Aspect of the structure on the coast of the West Greenland volcanic province reveled in seismic data. Bull. Geol. Soc. Denmark 55, 65–80.

Skaarup, N., Jackson, H.R., Oakey, G., 2006. Margin segmentation of Baffin Bay/Davis Strait, eastern canada based on seismic reflection and potential field data. Mar. Petrol. Geol., 23, 127–144.

Stica, J.M., Zalán, P.V., Ferrari, A.L., 2014. The evolution of rifting on the volcanic margin of the Pelotas Basin and the contextualization of the Paraná–Etendeka LIP in the separation of Gondwana in the South Atlantic. Mar. and Petrol. Geol. 50, 1-21.

Storey, M., Duncan, R.A., Pedersen, A.K., Larsen, L.M., Larsen, H.C., 1998. 40Ar/39Ar geochronology of the West Greenland Tertiary volcanic province. Earth and Planetary Science Letters 160, 569–586.

Suckro, S., Gohl, K., Funck, T., Heyde, I., Ehrhardt, A., Schreckenberger, B., Gerlings, J., Damm, V., Jokat, W., 2012. The crustal structure of southern Baffin Bay: implications from a seismic refraction experiment. Geophys. J. Int., 190, 37–58.

Suckro, S., Gohl, K., Funck, T., Heyde, I., Schreckenberger, B., Gerlings, J., Damm, V., 2013. The davis strait crust – a transform margin between two oceanic basins. Geophys. J. Int., 193, 78–97.

Watt, W.S., 1969. The coast-parallel dike swarm of southwest Greenland in relation to the opening of the Labrador Sea. Canadian Journal of Earth Sciences 6, 1320-1321.

Welford, J.K., Peace, A.L., Geng, M., Dehler, S.A., Dickie, K., 2018. Crustal structure of Baffin Bay from constrained 3-D gravity inversion and deformable plate tectonic models. Geophys. J. Int. 142.

White, R.S., Spence, G.D., Fowler, S.R., McKenzie, D.P., Westbrook, G.K., Bowen, A.N., 1987. Magmatism at rifted continental margins. Nature 330, 439-444.

White, R. S., White, D., O'Nions, R. K., 1992. Oceanic crustal thickness from seismic measurements and rare earth element inversions. J. Geophys. Res., 97, 19,683– 19,715, doi:10.1029/92JB01749.

Whittaker, R.C., Hamann, N.E., Pulvertaft, T.C.R., 1997. A new frontier province offshore northern West Greenland: structure, basin development and petroleum potential of the Melville Bay area. Am. Assoc. Petrol. Geol. Bull. 81, 979–998.

Williamson, M.-C., Villeneuve, M.E., Larsen, L.M., Jackson, H.R., Oakey, G.N. & MacLean, B., 2001. Age and petrology of offshore basalts from the southeast Baffin Shelf, Davis Strait, and western Greenland continental margin. Geological Association of Canada & Mineralogical Association of Canada (GCA/MAC) Annual Meeting, St. John's, New Foundland, Canada, 27–30 May 2001, Abstract volume 26, 162 only.

Figure captions

Figure 1. Regional bathymetric, geological and tectonic framework. (a) The North Atlantic Igneous Province (modified from Larsen and Saunders, 1998). (b) Bathymetry of the Labrador Sea, Davis Strait and Baffin Bay (GEBCO_08 Grid, http://www.gebco.net). The Greenland Plate motion path relative to the North American Plate is shown as black lines and squares for 3 locations of the Greenland coast at magnetochrons C27 to C13 (from Oakey and Chalmers, 2012). The northward reorganization started at C25 (late Paleocene). CD: Cape Dyer, D: Disko, N: Nuussuaq, S: Svartenhuk. (c) Geological map of the Labrador-Baffin margins and oceanic domains modified after Chalmers and Oakey (2007) and Oakey and Chalmers (2012). SDR mapping from Keen et al. (2012), Skaarup et al. (2006), Funck et al. (2012), Suckro et al. (2012) and Abdelmalak et al. (2018). UFZ and HFZ: Ungava and Hudson fault zones respectively; DSH: Davis Straigth High. Seismic refraction lines from: (1) Funck et al. (2007); (2) Gerlings et al. (2009); (3) Suckro et al. (2013); (4) Funck et al. (2012); (5) Suckro et al. (2012). Orange circles: well locations where Paleogene volcanics were drilled: (a) Delta-1, (b) Hellefisk-1, (c) Nukik-2, (d) Gjoa G-37, (e) Ralegh N-18, (f) Hekja O-71. UE : Upernavik Escarpement.

Figure 2. Stratigraphic columns and major tectonic events from the Labrador (Hopedale and Saglek) basins, southern West Greenland offshore basins and the Nuussuaq Basin onshore central West Greenland. Stratigraphic columns are modified from Chalmers (2012). "*DSH transpression*" applies to the folding phase recorded along the Davis Strait High (Fig. 1c) after the N-S kinematic reorganization of the Labrador seafloor spreading. In Nuussuaq basin, volcanic formations are V: Vaigat, M: Maligat, S: Svartenhuk, N: Naqerloq, E: Erqa.

Figure 3. Free air gravity (a) and magnetic (b) anomalies over Baffin Bay and Davis Strait. Free air anomaly is from Sandwell et al. (2014) and the magnetic anomaly at sea-level grid is from Meyer et al. (2017) EMAG2-V3. The linear gravity lows are interpreted as extinct spreading centers in the Baffin Bay (Whittaker et al., 1997). Their location and the extent of the Eocene and Paleocene oceanic crust domains according to Oakey and Chalmers (2012) are also reported on the magnetic grid.

Figure 4. Simplified geological map (a) of West Greenland (adapted from Abdelmalak et al., 2012) showing the locations of available palaeomagnetic data (white circles) and dated rock samples (colored dots). Riisager et al. (2003) palaeomagnetic profiles 1-4 are from the Vaigat Fm., profile 5 from the Maligat Fm., profile 6 from the Kanisut Mb. (b) Stratigraphy and ages of the Tertiary volcanic succession according to Larsen et al. (2015).

Figure 5. Geological map and structure of Svartenhuk Peninsula, modified from Larsen (1983) and Larsen and Grocott (1992). The cross-sections illustrate the structure of the Tertiary volcanic successions along profiles AA', BB' and CC'. CBF: Cretaceous basin Boundary Fault.

Figure 6. Selected views of the Svartenhuk inner-SDR structure. The inset map (same legend as for Fig. 3) shows the location and orientation of each panorama. A.F.: Arfertuarssuk Fault. (a) Helicopter view of the crustal flexure which developed in the hanging wall of the A.F. (b) Example of a tilted continentward-dipping normal fault and associated splay faults within the V2 unit (southern coast of Svartenhuk Halvø). (c) Eroded V4 lavas dipping towards the Arfertuarssuk Fault. In the background, V3 unit lava outcrop along the fault footwall. (d) 3D view (Spot 6 images draped on the Aster DEM) of the A.F. hanging wall with V3 and V4 units tilted SW-ward (i.e. oceanward).

Figure 7. Location maps of samples used for radiometric dating and palaeomagnetic studies (a. basaltic flows; b. planar intrusions). Ages reported in whites boxes are $^{40}Ar/^{39}Ar$ ages ($\pm 2\sigma$). Zones I to VI refer to sampling areas. The dykes are mapped from Spot 6 satellite images. (c) Stratigraphy of the Svartenhuk lavas based on $^{40}Ar/^{39}Ar$ and K-Ar ages.

Figure 8. Paleomagnetic results. (a) and (b) Pilot demagnetization (15 steps) of samples from flows and dykes, respectively. (c) to (f) Representative demagnetization diagrams obtained using stepwise thermal demagnetization. Black (white) circles represent projections onto the horizontal (vertical) plane. Dashed lines indicate the best fit line obtained using principal component analysis. The declination, inclination, and maximum angular deviation (MAD) values are given for each of these fits. Gray symbols on the diagram reported in f illustrate the viscous component removed after the very first demagnetization steps.

Figure 9. Stereoplots of the characteristic remanent magnetization (ChRM) mean directions obtained from stepwise demagnetizations of (a) flows and (b) dykes. The mean directions calculated using the Fisher statistics are reported as blue crosses and the red circles show the ellipse of confidence (α_{95}). The average directions obtained by Riisager et al. (2003) in the Svartenhuk Halvo V1 unit and in the Kanisut Mb. of Nuussuaq are plotted for comparison. (c) Variations in the flow-mean paleomagnetic directions, bottom to top, in Svartenhuk lavas. The average declinations and inclinations calculated from all data correspond to the gray shaded lines. The y axis refers to the relative position of samples along the southern coast of Svartenhuk (see Fig. 5a for location).

Figure 10. Synthesis of ages obtained from flows and intrusions of the Western Greenland Volcanic Province, from the southern Davis Strait to central West Greenland. Time scale is from Ogg (2012). Ages are plotted with confidence interval of +/- 1σ. In each area, data are displayed from the left to right as a function of stratigraphic order. VF - Vaigat Formation, MF - Maligât Formation. SF – Svartenhuk Formation, Na - Naujánguit Mb., Or - Ordlingassoq Mb., RD - Rinks Dal Mb., No - Nordfjord Mb. & Niaqussat Mb. (Nunavik unit), Ka - Kanísut Mb., SF LM and SF UM – Lower and Upper Mb. of the Svartenhuk Formation; (1) Storey et al. (1998) ages modified by Skaarup and Pulvertaft (2007); (2) Larsen et al. (2015); (3) Geoffroy et al. (2001) mean age calculated from 5 different dykes; (4) Williamson et al. (2001); (5) Nelson et al. (2015).

Figure 11. Structure of the Tertiary volcanics to the west of the Itilli fault in the Nuussuaq peninsula. Insert: location of the profiles. See also Fig. 4.

Figure 12. Age versus structural attitude of dykes sampled in the Svartenhuk Halvø. Uncertainties for K-Ar and $^{40}Ar/^{39}Ar$ ages are given at the 2σ level. Strikes and dips of dykes are shown between brackets.

Figure 13. Baffin Bay crustal models. (a) Oakey and Chalmers (2012)'s crustal model of Fig. 1c compared with crustal thickness within Baffin Bay derived from gravity inversion models; (b) Hosseinpour et al. (2013); (c) Welford et al. (2018).

Table caption

Table 1. (a) Details of replicate analyses and K/Ar age determinations (shown in stratigraphic order). Values reported with an asterisk have not been included in the data analysis. Strike/dip of dykes are indicated in brackets. (b) Summary of $^{40}Ar/^{39}Ar$ data from incremental heating experiments. Ages are calculated relative to the 28.201 Ma Fish Canyon sanidine standard.

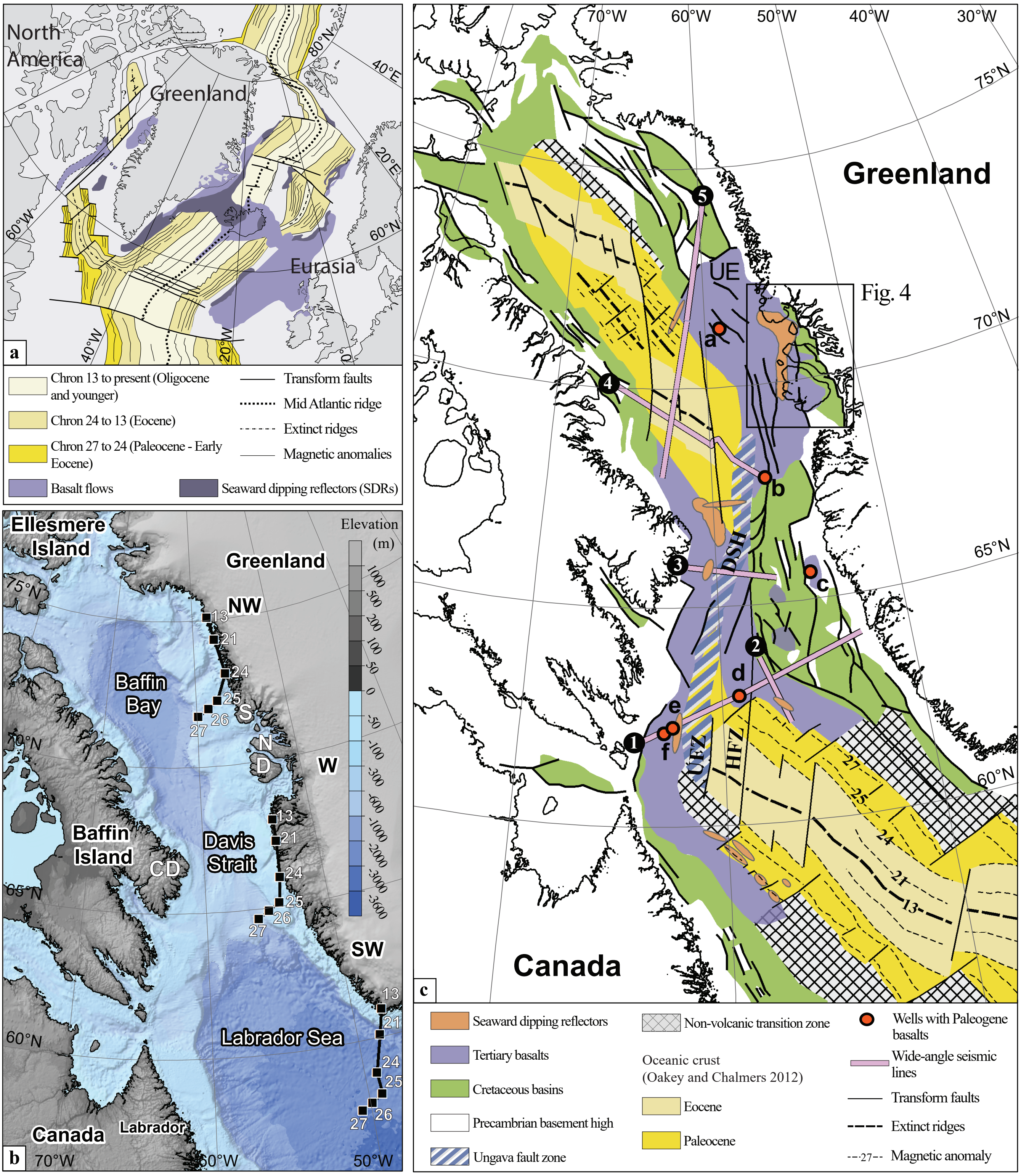

North America
Greenland
Eurasia
80°N
40°E
20°E
60°N
60°W
40°W
20°W
0°
a
Chron 13 to present (Oligocene and younger)
Chron 24 to 13 (Eocene)
Chron 27 to 24 (Paleocene - Early Eocene)
Basalt flows
Transform faults
Mid Atlantic ridge
Extinct ridges
Magnetic anomalies
Seaward dipping reflectors (SDRs)
Ellesmere Island
Greenland
Elevation (m)
1000
500
200
100
50
0
-50
-100
-300
-600
-1000
-2000
-3000
-3600
75°N
70°N
65°N
60°N
NW
Baffin Bay
S
N
D
W
Baffin Island
CD
Davis Strait
SW
Labrador Sea
Canada
Labrador
70°W
60°W
50°W
b
70°W
60°W
50°W
40°W
30°W
75°N
70°N
65°N
60°N
Greenland
Fig. 4
UE
DSH
UFZ
HFZ
Canada
c
Seaward dipping reflectors
Tertiary basalts
Cretaceous basins
Precambrian basement high
Ungava fault zone
Non-volcanic transition zone
Oceanic crust (Oakey and Chalmers 2012)
Eocene
Paleocene
Wells with Paleogene basalts
Wide-angle seismic lines
Transform faults
Extinct ridges
--27-- Magnetic anomaly

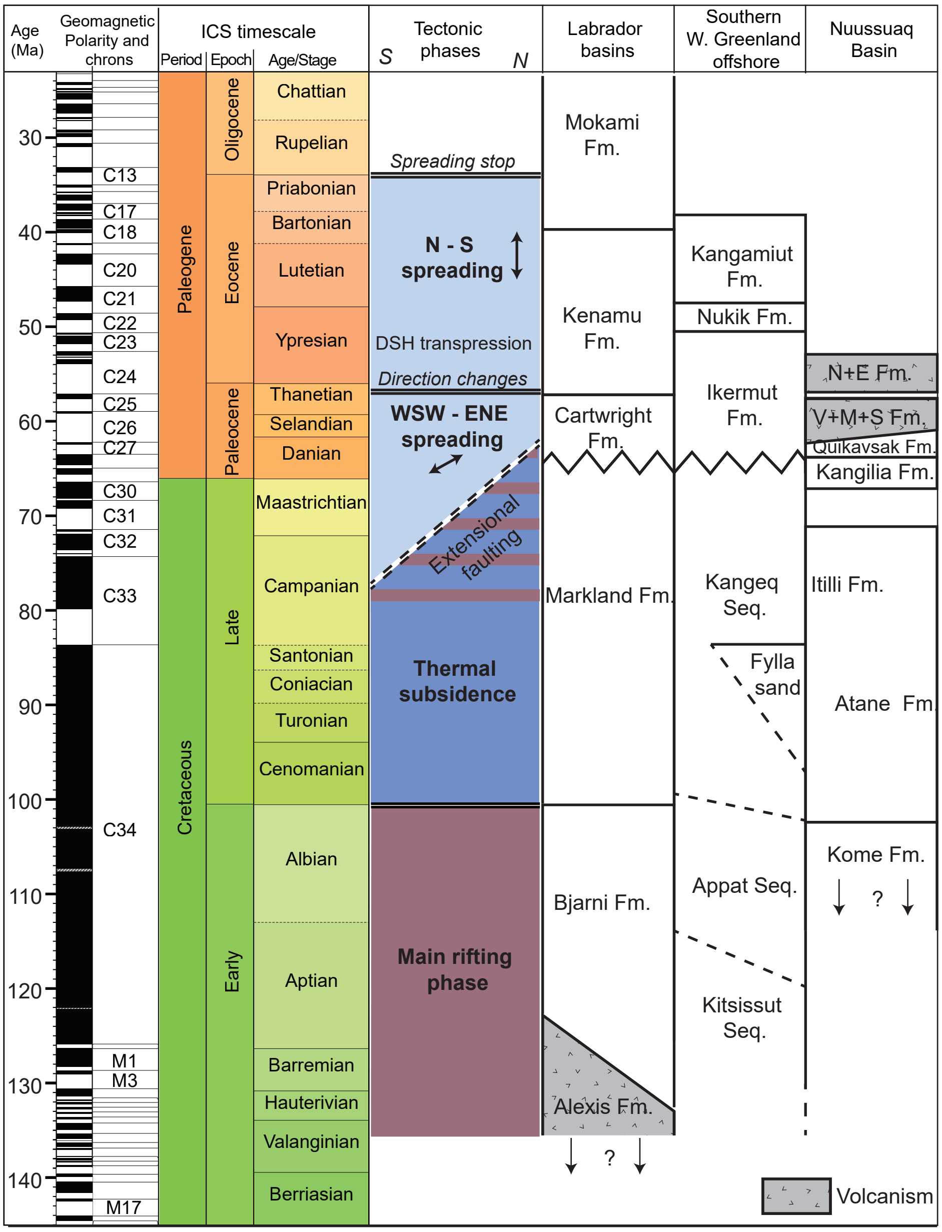
Age (Ma)
Geomagnetic Polarity and chrons
ICS timescale
Period
Epoch
Age/Stage
Tectonic phases
S
N
Labrador basins
Southern W. Greenland offshore
Nuussuaq Basin
30
40
50
60
70
80
90
100
110
120
130
140
C13
C17
C18
C20
C21
C22
C23
C24
C25
C26
C27
C30
C31
C32
C33
C34
M1
M3
M17
Paleogene
Cretaceous
Oligocene
Eocene
Paleocene
Late
Early
Chattian
Rupelian
Priabonian
Bartonian
Lutetian
Ypresian
Thanetian
Selandian
Danian
Maastrichtian
Campanian
Santonian
Coniacian
Turonian
Cenomanian
Albian
Aptian
Barremian
Hauterivian
Valanginian
Berriasian
Spreading stop
N - S spreading
DSH transpression
Direction changes
WSW - ENE spreading
Extensional faulting
Thermal subsidence
Main rifting phase
Mokami Fm.
Kenamu Fm.
Cartwright Fm.
Markland Fm.
Bjarni Fm.
Alexis Fm.
?
Kangamiut Fm.
Nukik Fm.
Ikermut Fm.
Kangeq Seq.
Fylla sand
Appat Seq.
Kitsissut Seq.
N+E Fm.
V+M+S Fm.
Quikavsak Fm.
Kangilia Fm.
Itilli Fm.
Atane Fm.
Kome Fm.
?
Volcanism

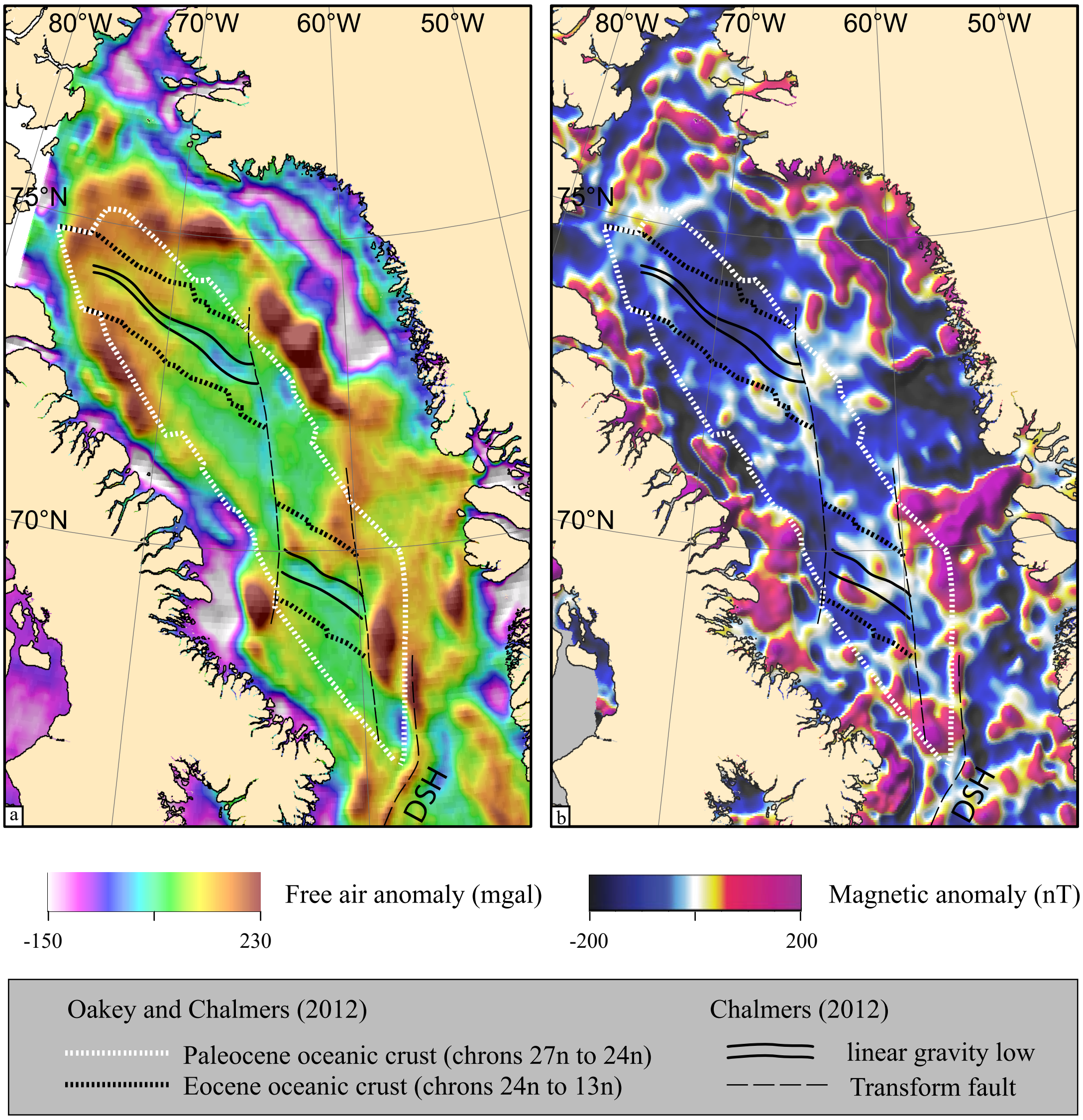
80°W
70°W
60°W
50°W
75°N
70°N
DSH
a
b
Free air anomaly (mgal)
-150
230
Magnetic anomaly (nT)
-200
200
Oakey and Chalmers (2012)
Paleocene oceanic crust (chrons 27n to 24n)
Eocene oceanic crust (chrons 24n to 13n)
Chalmers (2012)
linear gravity low
Transform fault

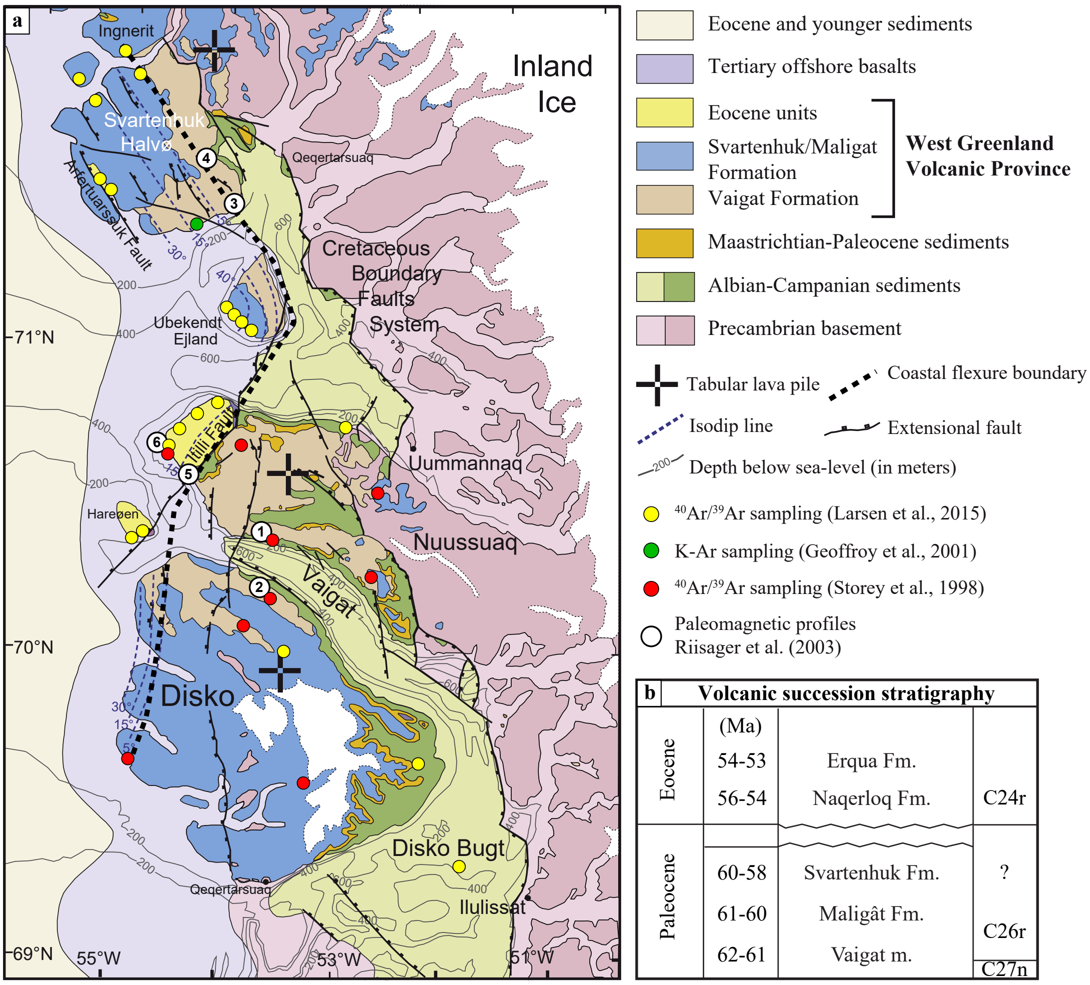
a
Ingnerit
Svartenhuk Halvø
Arfertuarssuk Fault
Qeqertarsuaq
Inland Ice
Cretaceous Boundary Faults System
Ubekendt Ejland
Itilli Fault
Hareøen
Uummannaq
Nuussuaq
Vaigat
Disko
Disko Bugt
Ilulissat
71°N
70°N
69°N
55°W
53°W
51°W
Eocene and younger sediments
Tertiary offshore basalts
Eocene units
Svartenhuk/Maligat Formation
Vaigat Formation
West Greenland Volcanic Province
Maastrichtian-Paleocene sediments
Albian-Campanian sediments
Precambrian basement
Tabular lava pile
Coastal flexure boundary
Isodip line
Extensional fault
Depth below sea-level (in meters)
40Ar/39Ar sampling (Larsen et al., 2015)
K-Ar sampling (Geoffroy et al., 2001)
40Ar/39Ar sampling (Storey et al., 1998)
Paleomagnetic profiles Riisager et al. (2003)
b
Volcanic succession stratigraphy
Eocene
(Ma)
54-53
Erqua Fm.
56-54
Naqerloq Fm.
C24r
Paleocene
60-58
Svartenhuk Fm.
?
61-60
Maligât Fm.
C26r
62-61
Vaigat m.
C27n

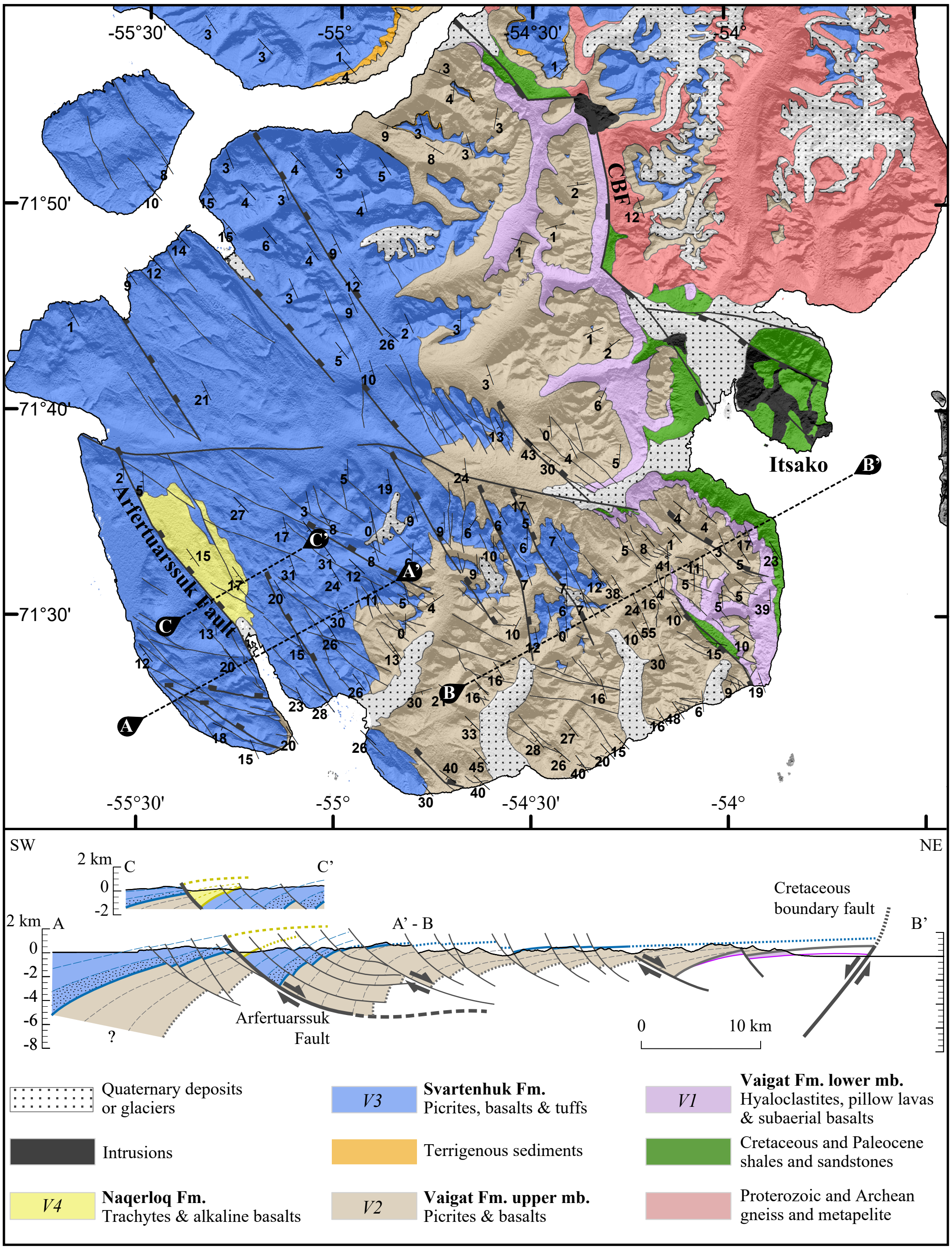

-55°30'
-55°
-54°30'
-54°
71°50'
71°40'
71°30'
CBF
Itsako
Arfertuarssuk Fault
A
A'
B
B'
C
C'
SW
NE
2 km
0
-2
-4
-6
-8
A' - B
Cretaceous boundary fault
Arfertuarssuk Fault
?
0
10 km
Quaternary deposits or glaciers
Intrusions
V4 Naqerloq Fm. Trachytes & alkaline basalts
V3 Svartenhuk Fm. Picrites, basalts & tuffs
Terrigenous sediments
V2 Vaigat Fm. upper mb. Picrites & basalts
V1 Vaigat Fm. lower mb. Hyaloclastites, pillow lavas & subaerial basalts
Cretaceous and Paleocene shales and sandstones
Proterozoic and Archean gneiss and metapelite

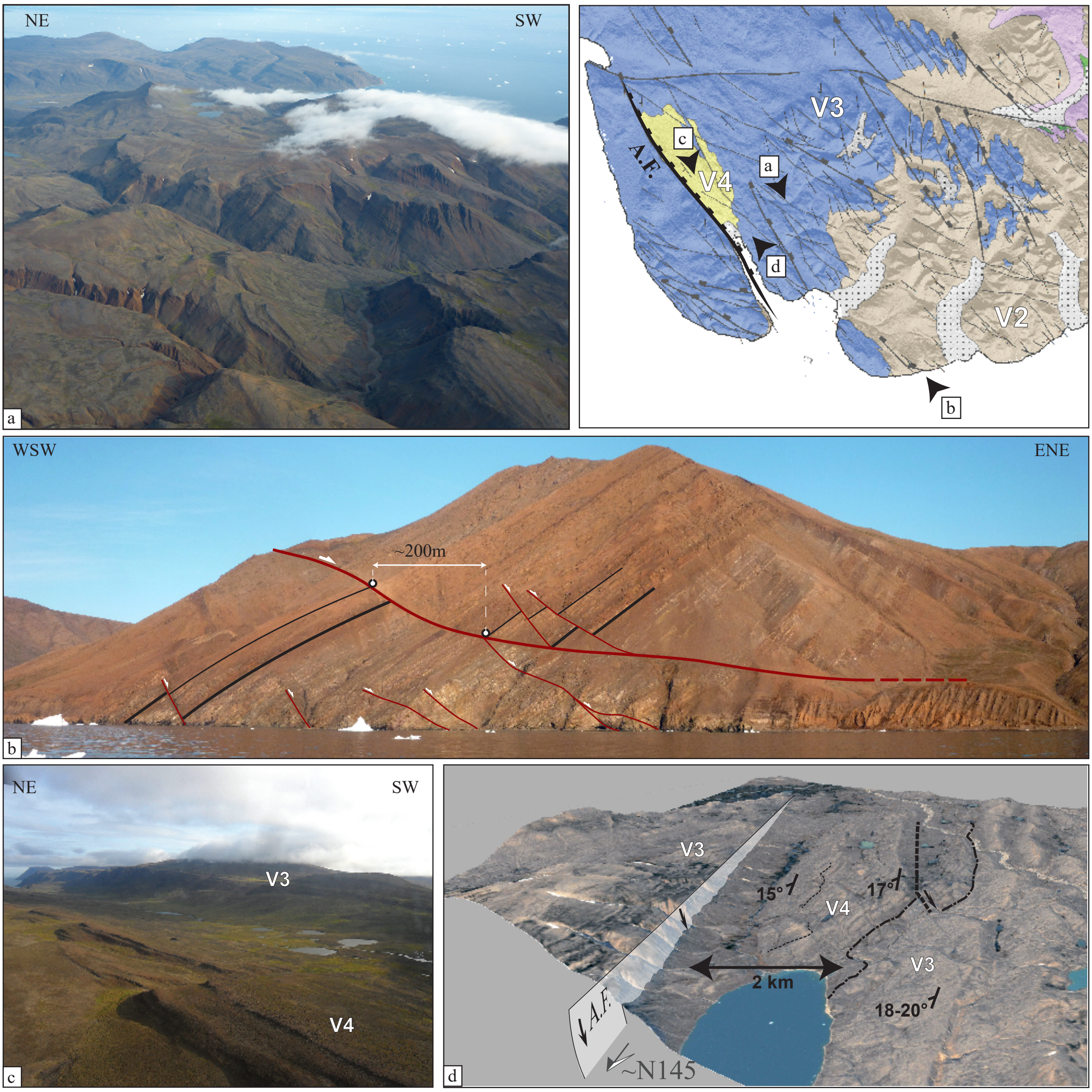
NE
SW
a
V3
c
A.F.
V4
a
d
V2
b
WSW
ENE
~200m
b
NE
SW
V3
V4
c
V3
15°
17°
V4
2 km
V3
18-20°
A.F.
~N145
d

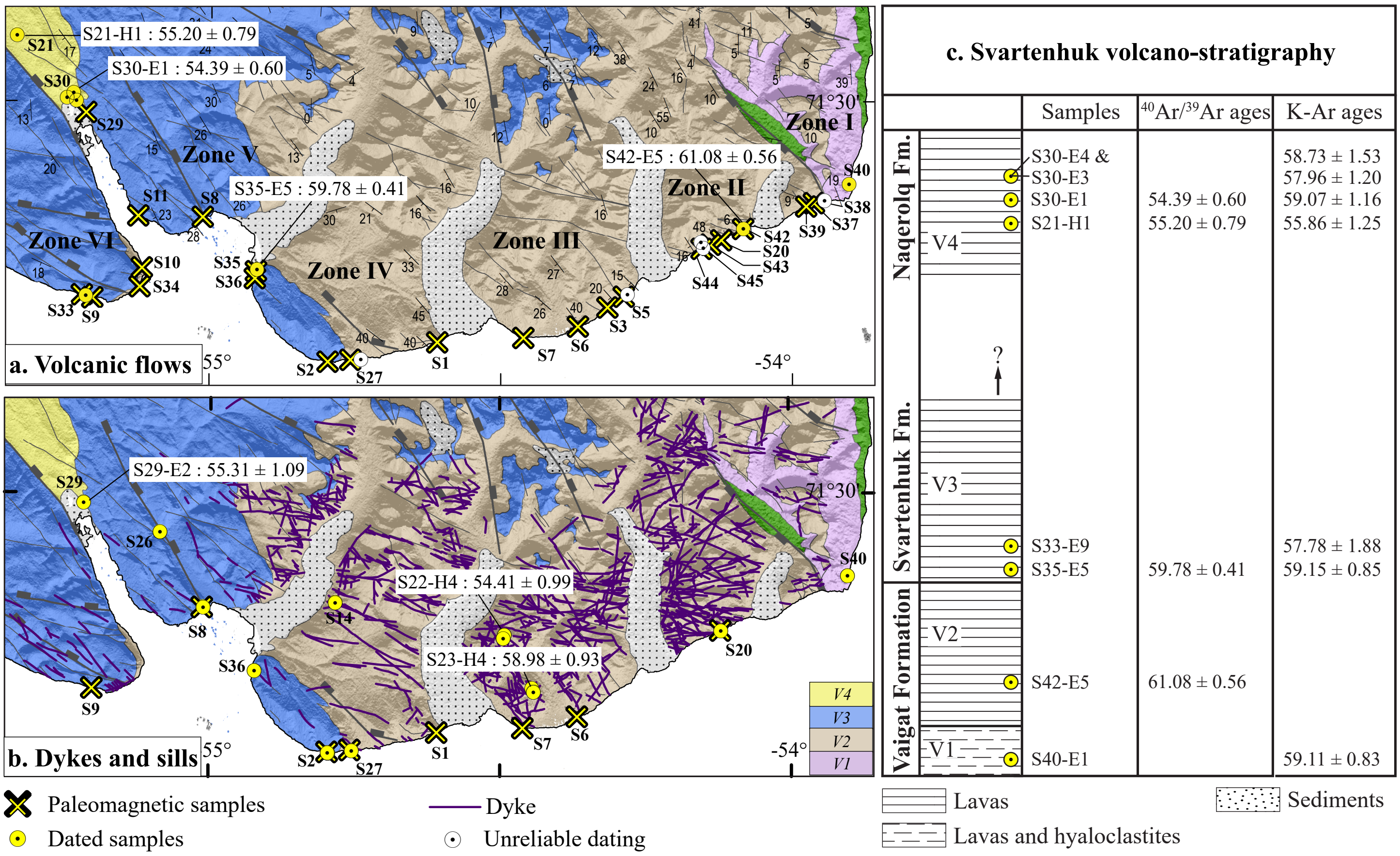
a. Volcanic flows
b. Dykes and sills
c. Svartenhuk volcano-stratigraphy
Zone I
Zone II
Zone III
Zone IV
Zone V
Zone VI
S21-H1 : 55.20 ± 0.79
S30-E1 : 54.39 ± 0.60
S35-E5 : 59.78 ± 0.41
S42-E5 : 61.08 ± 0.56
S29-E2 : 55.31 ± 1.09
S22-H4 : 54.41 ± 0.99
S23-H4 : 58.98 ± 0.93
71°30'
55°
-54°
V4
V3
V2
V1
Samples
$^{40}Ar/^{39}Ar$ ages
K-Ar ages
Naqerolq Fm.
Svartenhuk Fm.
Vaigat Formation
S30-E4 &
S30-E3
S30-E1
S21-H1
S33-E9
S35-E5
S42-E5
S40-E1
54.39 ± 0.60
55.20 ± 0.79
59.78 ± 0.41
61.08 ± 0.56
58.73 ± 1.53
57.96 ± 1.20
59.07 ± 1.16
55.86 ± 1.25
57.78 ± 1.88
59.15 ± 0.85
59.11 ± 0.83
Paleomagnetic samples
Dated samples
Dyke
Unreliable dating
Lavas
Lavas and hyaloclastites
Sediments

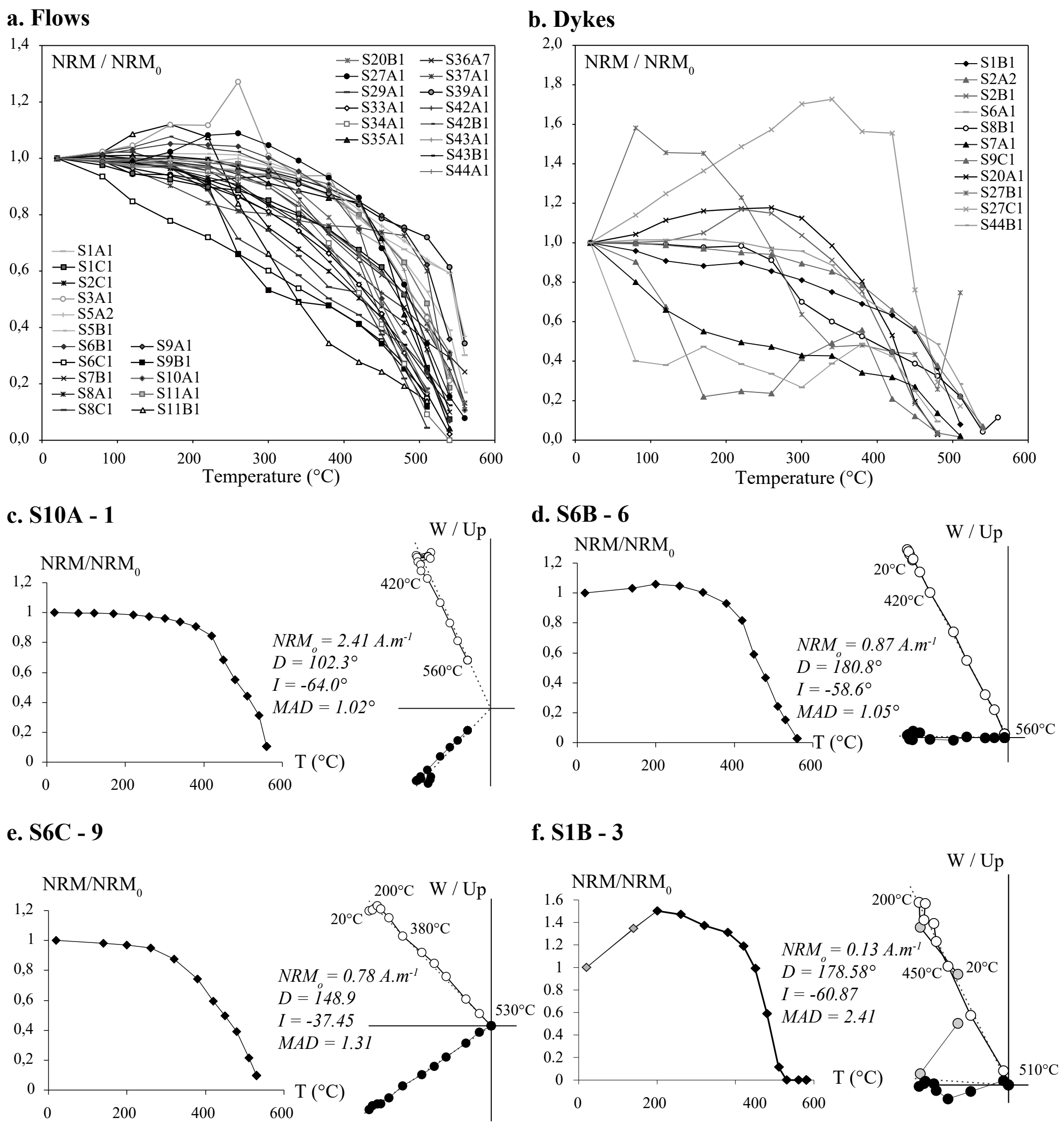

a. Flows
NRM / NRM0
S20B1
S27A1
S29A1
S33A1
S34A1
S35A1
S36A7
S37A1
S39A1
S42A1
S42B1
S43A1
S43B1
S44A1
S1A1
S1C1
S2C1
S3A1
S5A2
S5B1
S6B1
S6C1
S7B1
S8A1
S8C1
S9A1
S9B1
S10A1
S11A1
S11B1
Temperature (°C)
b. Dykes
NRM / NRM0
S1B1
S2A2
S2B1
S6A1
S8B1
S7A1
S9C1
S20A1
S27B1
S27C1
S44B1
Temperature (°C)
c. S10A - 1
NRM/NRM0
T (°C)
W / Up
420°C
560°C
NRMo = 2.41 A.m-1
D = 102.3°
I = -64.0°
MAD = 1.02°
d. S6B - 6
NRM/NRM0
T (°C)
W / Up
20°C
420°C
560°C
NRMo = 0.87 A.m-1
D = 180.8°
I = -58.6°
MAD = 1.05°
e. S6C - 9
NRM/NRM0
T (°C)
W / Up
200°C
20°C
380°C
530°C
NRMo = 0.78 A.m-1
D = 148.9
I = -37.45
MAD = 1.31
f. S1B - 3
NRM/NRM0
T (°C)
W / Up
200°C
450°C
20°C
510°C
NRMo = 0.13 A.m-1
D = 178.58°
I = -60.87
MAD = 2.41

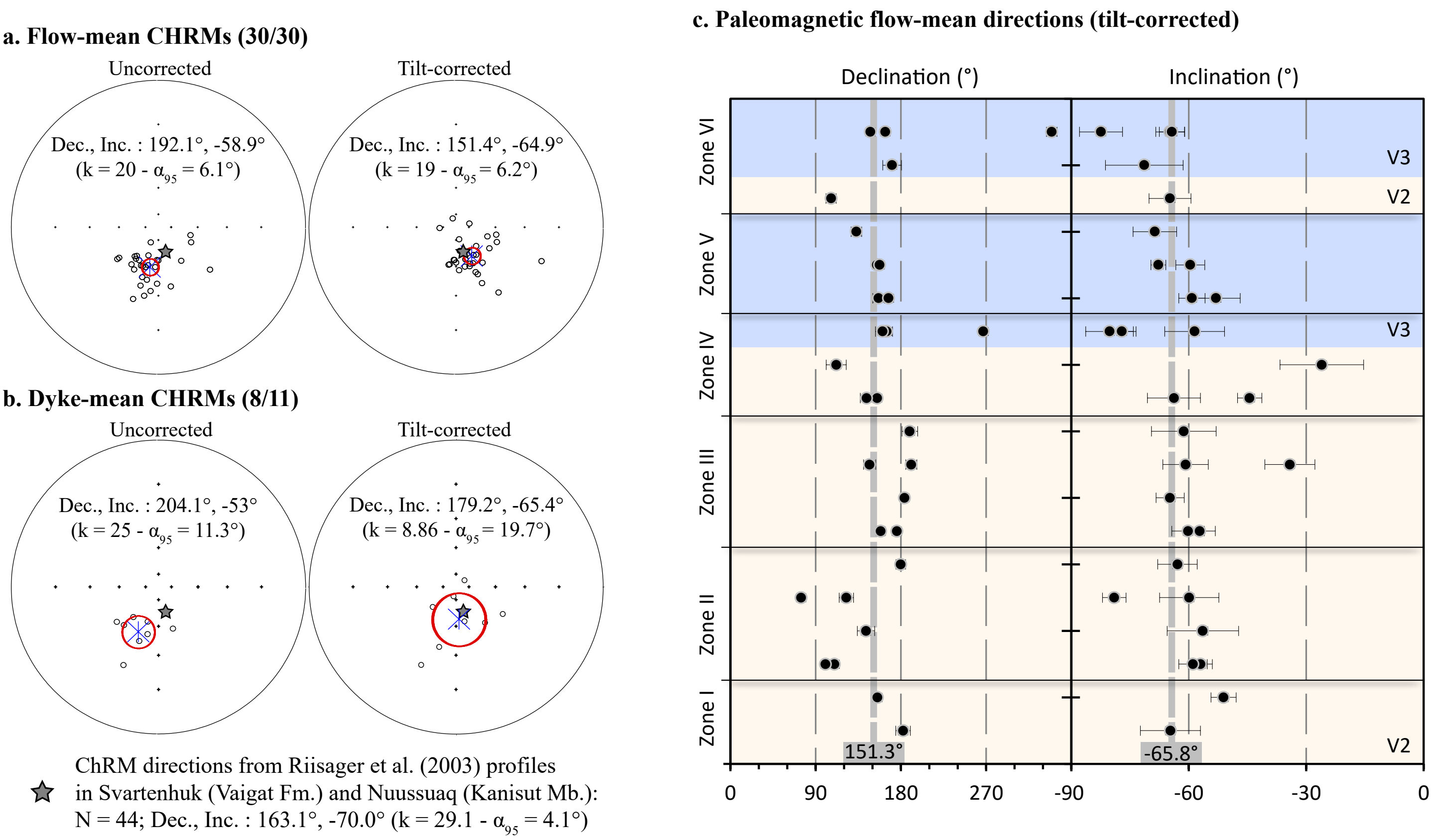

a. Flow-mean CHRMs (30/30)
Uncorrected
Dec., Inc. : 192.1°, -58.9°
(k = 20 - α_{95} = 6.1°)
Tilt-corrected
Dec., Inc. : 151.4°, -64.9°
(k = 19 - α_{95} = 6.2°)
b. Dyke-mean CHRMs (8/11)
Uncorrected
Dec., Inc. : 204.1°, -53°
(k = 25 - α_{95} = 11.3°)
Tilt-corrected
Dec., Inc. : 179.2°, -65.4°
(k = 8.86 - α_{95} = 19.7°)
ChRM directions from Riisager et al. (2003) profiles in Svartenhuk (Vaigat Fm.) and Nuussuaq (Kanisut Mb.): N = 44; Dec., Inc. : 163.1°, -70.0° (k = 29.1 - α_{95} = 4.1°)
c. Paleomagnetic flow-mean directions (tilt-corrected)
Declination (°)
Inclination (°)
Zone VI
Zone V
Zone IV
Zone III
Zone II
Zone I
V3
V2
V3
V2
151.3°
-65.8°
0
90
180
270
-90
-60
-30
0

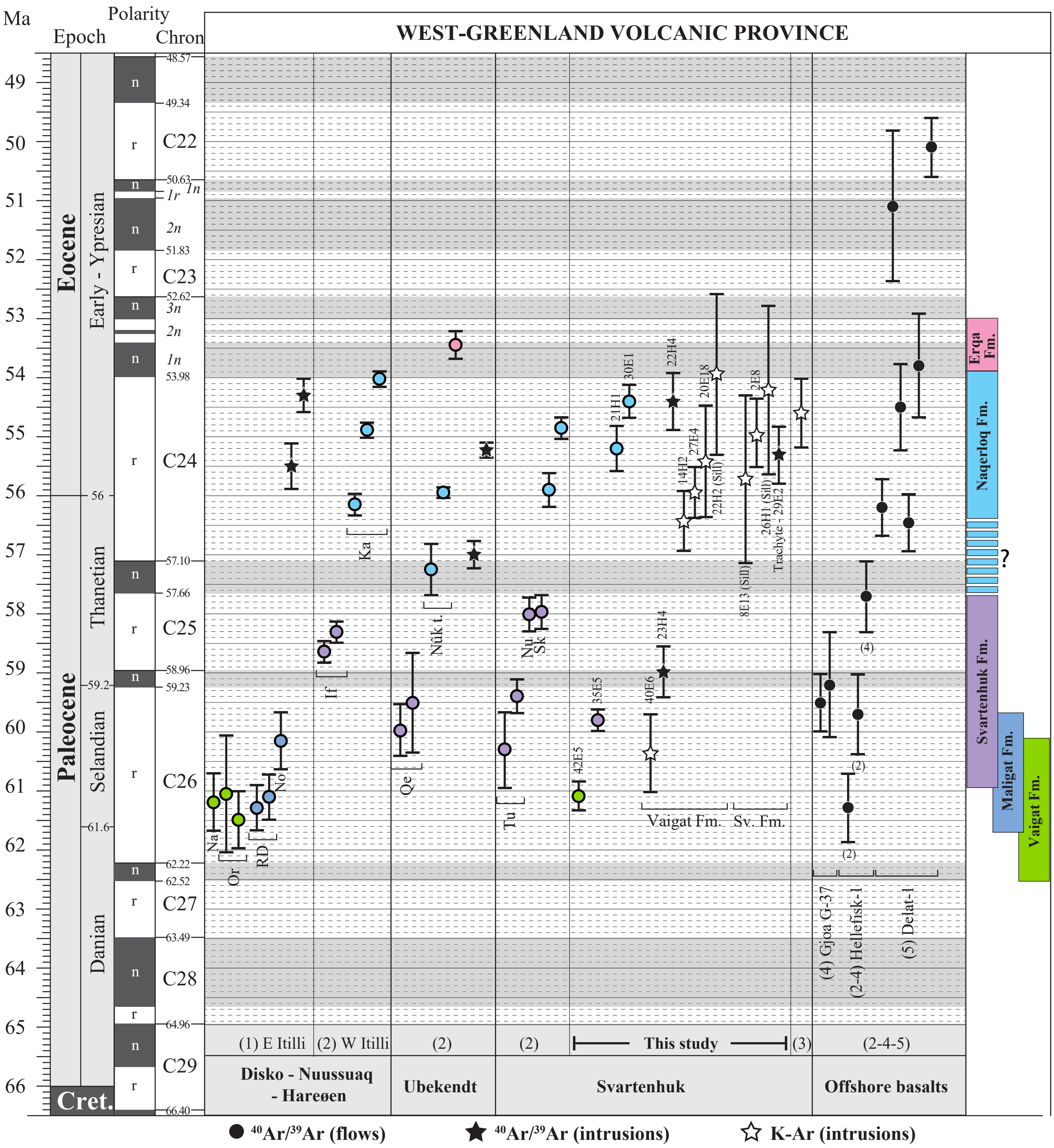

WEST-GREENLAND VOLCANIC PROVINCE
Ma
Epoch
Polarity
Chron
Eocene
Early - Ypresian
Paleocene
Thanetian
Selandian
Danian
Cret.
C22
C23
C24
C25
C26
C27
C28
C29
Disko - Nuussuaq - Hareøen
Ubekendt
Svartenhuk
Offshore basalts
(1) E Itilli
(2) W Itilli
(2)
(2)
This study
(3)
(2-4-5)
Vaigat Fm.
Sv. Fm.
(4) Gjoa G-37
(2-4) Hellefisk-1
(5) Delat-1
Erqa Fm.
Naqerloq Fm.
Svartenhuk Fm.
Maligat Fm.
Vaigat Fm.
$^{40}Ar/^{39}Ar$ (flows)
$^{40}Ar/^{39}Ar$ (intrusions)
K-Ar (intrusions)

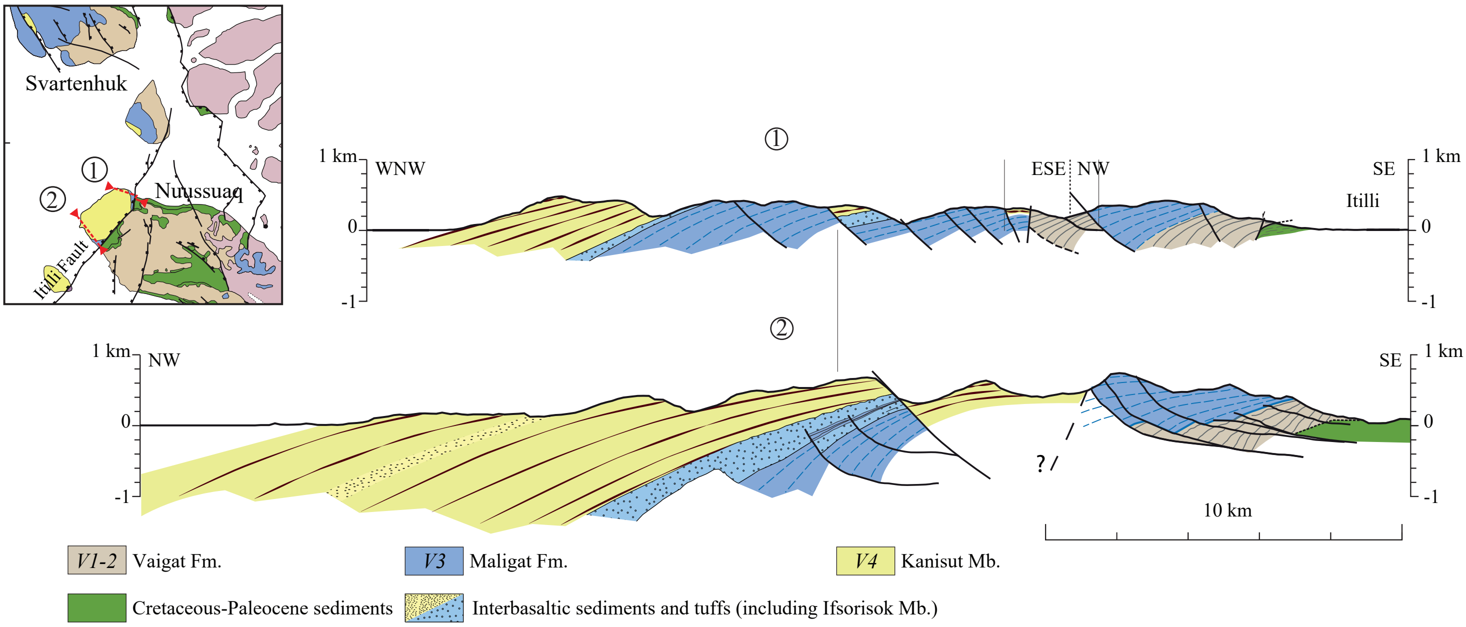

Svartenhuk
①
②
Nuussuaq
Itilli Fault
1 km
WNW
ESE
NW
SE
Itilli
0
-1
1 km
NW
SE
?
10 km
V1-2 Vaigat Fm.
V3 Maligat Fm.
V4 Kanisut Mb.
Cretaceous-Paleocene sediments
Interbasaltic sediments and tuffs (including Ifsorisok Mb.)

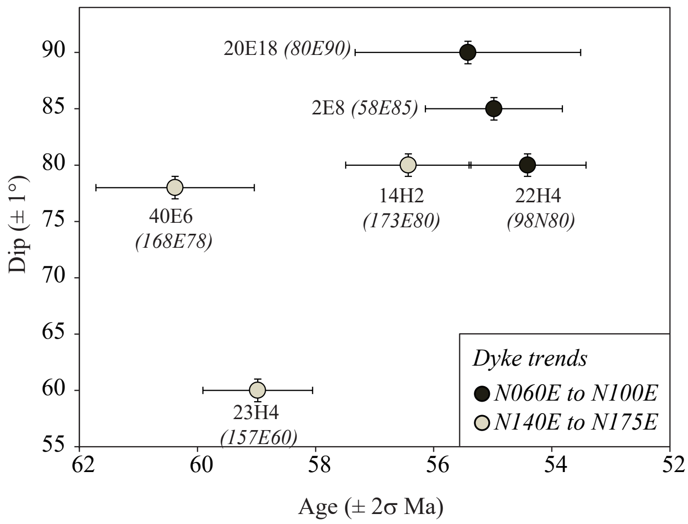

20E18 (80E90)
2E8 (58E85)
40E6
(168E78)
14H2
(173E80)
22H4
(98N80)
23H4
(157E60)
Dyke trends
N060E to N100E
N140E to N175E
Dip (± 1°)
Age (± 2σ Ma)
90
85
80
75
70
65
60
55
62
60
58
56
54
52

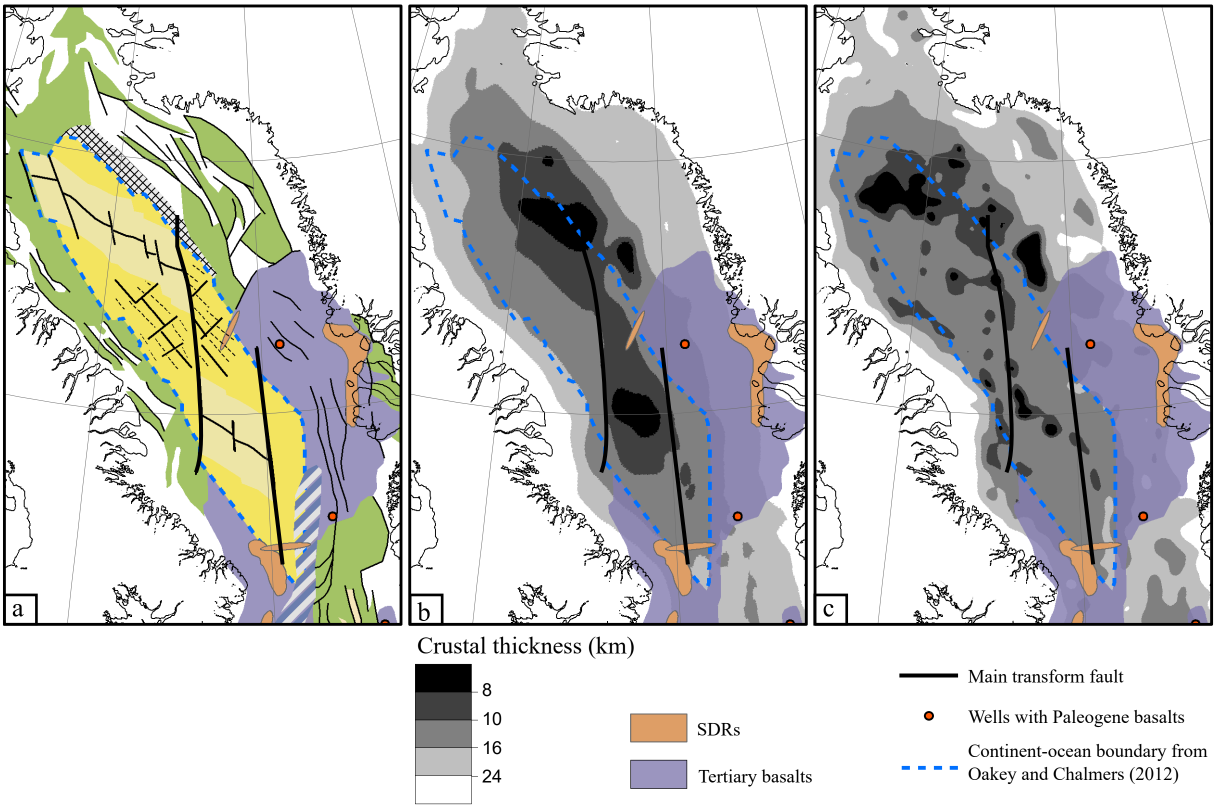
a
b
c
Crustal thickness (km)
8
10
16
24
SDRs
Tertiary basalts
Main transform fault
Wells with Paleogene basalts
Continent-ocean boundary from
Oakey and Chalmers (2012)

Table 1. (a) Details of replicate analyses and K/Ar age determinations (classified in a stratigraphic order).Values reported with an asterisk have not been taken into account. Strike/dip of dykes is indicated in brackets. (b) Summary of $^{40}Ar/^{39}Ar$ data from incremental heating experiments. Ages are calculated relative to the 28.201 Ma Fish Canyon sanidine standard.

a. K/Ar

Sample	*Lat. (°N)*	*Long. (°W)*	Experiment no.	K (wt%) ± 1 σ	Mass molten (g)	$^{40}Ar^*$ (%)	$^{40}Ar^*$ (10^{-11} mol./g) ± 1 σ	$^{40}Ar^*$ weighted mean (10^{-11} mol./g) ± 1 σ	Age (Ma) ± 2 σ
Flow									
S40-E1			8631	0.470 ± 0.003	0.32556	41.975	4.863 ± 0.024		
	71,45477	*53,89866*	8647	« ………….. »	0.31922	34.937	4.933 ± 0.025	4.898 ± 0.018	**59.11 ± 0.83***
S35-E5			8629	0.428 ± 0.004	0.30871	63.746	4.461 ± 0.023		
	71,40867	*54,91839*	8677	« ………….. »	0.31594	26.988	4.524 ± 0.023		
			8716	« ………….. »	0.31737	51.665	4.407 ± 0.22	4.463 ± 0.013	**59.15 ± 0.85**
S33-E9			8634	0.205 ± 0.004	0.34632	61.668	2.083 ± 0.011		
	71,39358	*55,21253*	8650	« ………….. »	0.50091	50.705	2.091 ± 0.011	2.087 ± 0.008	**57.78 ± 1.88***
S30-E1			8630	0.821 ± 0.013	0.32107	87.934	8.755 ± 0.043		
	71,50236	*55,24889*	8646	« ………….. »	0.37134	80.374	8.542 ± 0.042		
			8717	« ………….. »	0.41709	84.681	8.532 ± 0.043	8.550± 0.025	**59.07 ± 1.16***
S30-E3			8777	0.604 ± 0.008	0.30554	88.082	6.181 ± 0.031		
	71,50233	*55,24106*	8793	« ………….. »	0.30494	74.402	6.158 ± 0.031	6.169 ± 0.022	**57.96 ± 1.20***
S30-E4			8654	0.834 ± 0.014	0.29949	80.107	8.621 ± 0.043		
	71,50233	*55,24106*	8670	« ………….. »	0.2519	83.044	8.647 ± 0.043	8.634 ± 0.030	**58.73 ± 1.53***
S21-H1			8792	0.947 ± 0.013	0.29972	81.802	9.280 ± 0.046		
	71,53605	*55,33622*	8813	« ………….. »	0.38571	94.611	9.355 ± 0.047	9.317 ± 0.035	**55.86 ± 1.25**
Sill									
S22-H2			8800	0.136 ± 0.005	0.51055	22.029	1.310 ± 0.007		
	71,42281	*54,49116*	8806	« ………….. »	0.43979	17.128	1.268 ± 0.007	1.289 ± 0.005	**53.85 ± 2.84**
S36-E5			8635	0.222 ± 0.003	0.33573	39.503	2.468 ± 0.013		
	71,40308	*54,92181*	8651	« ………….. »	0.50249	40.015	2.480 ± 0.013		
			8714	« ………….. »	0.51316	35.472	2.448 ± 0.013	2.465 ± 0.007	**62.92 ± 0.92***
S26-H1			8628	0.228 ± 0.008	0.30007	30.645	2.185 ± 0.011		
	71,47894	*55,08561*	8644	« ………….. »	0.50213	40.288	2.167 ± 0.011	2.176± 0.008	**54.20 ± 2.88**
S8-E13			8805	0.190 ± 0.006	0.30856	22.17	1.856 ± 0.010		
	71,43780	*55,01043*	8821	« ………….. »	0.30692	65.418	1.873 ± 0.010	1.865 ± 0.007	**55.73 ± 2.49**
Dyke									
S40-E6			8773	0.556 ± 0.008	0.30171	22.037	5.959 ± 0.030		
	71,45472	*53,89972*	8789	« ………….. »	0.30652	23	5.881 ± 0.031	5.921 ± 0.021	**60.38 ± 1.34**
S14-H2			8782	0.764 ± 0.009	0.2251	76.085	7.475 ± 0.037		
	71,44078	*54,78275*	8798	« ………….. »	0.3026	59.493	7.721 ± 0.039	7.594 ± 0.027	**56.43 ± 1.06**
S27-E4			8823	0.519 ± 0.004	0.37472	76.323	5.092 ± 0.026		
	71,35933	*54,75433*	8839	« ………….. »	0.38755	71.082	5.137 ± 0.026	5.114 ± 0.018	**55.95 ± 0.88**
S20-E18			8657	0.654 ± 0.015	0.32671	37.396	6.431 ± 0.033		
	71,42483	*54,11903*	8673	« ………….. »	0.29308	58.455	6.338 ± 0.032	6.383 ± 0.023	**55.42 ± 1.91**
S2-E8			8781	0.621 ± 0.008	0.35445	78.369	5.892 ± 0.030		
	71,35819	*54,79525*	8797	« ………….. »	0.3219	57.36	6.145 ± 0.031	6.0122 ± 0.021	**54.98 ± 1.16**

b. $^{40}Ar/^{39}Ar$

Sample / **Experiment no.**	**wt. (mg)**	**K/Ca (total)**	**Total Fusion Age (Ma)**	**Increments used (°C)**	^{39}**Ar (%)**	**Isochron Analysis N**	**MSWD**	^{40}**Ar/**^{36}**Ar ± 2 σ intercept**	**Age ± 2 σ (Ma)**
Flow									
S42-E5, groundmass *(71,43083°N - 54,08153°W)*									
FG-1121 to FG-1129	101	0.06	60.00 ± 0.34	652-1016	80.9	7 of 9	1.08	293.4 ± 4.9	**61.08 ± 0.56**
S35-E5, groundmass *(71,40867°N - 54,91839°W)*									
FG-999 to FG-1009	138	0.12	59.60 ± 0.37	646-1098	100.0	11 of 11	1.59	293.2 ± 3.5	**59.78 ± 0.41**
S21-H1, groundmass *(71,53605°N - 55,33622°W)*									
FG-1151 to FG-1159	104	0.28	55.80 ± 0.76	839-1034	60.7	5 of 9	1.67	328.8 ± 114.0	**55.20 ± 0.79**
S30-E1, groundmass *(71,50236°N - 55,24889°W)*									
FG-1111 to FG-11120	106	0.34	55.46 ± 0.88	867-1100	70.3	5 of 9	1.89	307.9 ± 86.6	54.38 ± 0.90
FG-1140 to FG-1148	100	0.30	55.59 ± 0.79	898-1092	60.2	5 of 9	1.21	380.0 ± 105.0	54.40 ± 0.81
weighted mean plateau and isochron ages from two experiments:									**54.39 ± 0.60**
simple mean plateau and isochron ages from two experiments:									54.39 ± 0.86
Dyke									
S23-H4, groundmass ***(71,39363°N – 54,44445°W)***									
FG-1160 to FG-1171	101	0.10	58.79 ± 0.80	839-1085	66.7	6 of 11	2.10	295.3 ± 10.3	**58.98 ± 0.93**
S22-H4, groundmass ***(71,42121°N – 54,49360°W)***									
FG-1185 to FG-1195	106	0.24	54.74 ± 0.92	839-1225	86.5	8 of 11	1.60	300.5 ± 17.0	**54.41 ± 0.99**
Trachyte									
S29-E2, feldspars ***(71,49475°N - 55,21839°W)***									
N1268-01 to N1268-08						7 of 8	2.00	319.5 ± 99.0	**55.3 ± 1.09**